

Xiaoyu CUI
Tongyang LI
Shaoping WANG
Jian SHI
Zhonghai MA

RELIABILITY MODELING BASED ON POWER TRANSFER EFFICIENCY AND ITS APPLICATION TO AIRCRAFT ACTUATION SYSTEM

MODEL NIEZAWODNOŚCI OPARTY NA WYDAJNOŚCI PRZESYŁU ENERGII I JEGO ZASTOSOWANIE DO OCENY LOTNICZEGO UKŁADU HYDRAULIKI SIŁOWEJ

The power transfer systems (PTS) has special reliability properties, including multiple states and fault dependence. Consequently, traditional binary-state reliability modeling methods cannot accurately evaluate the reliability of PTS. In order to resolve the contradiction between terminal energy demand and power transfer capability of PTS, this paper proposes a novel multi-state reliability model based on power transfer efficiency (PTE) for reliability evaluation of PTS. The multi-state model caused by performance degradation based on PTE is considered in this paper. In addition, the failure correlation in virtue of the system structure and energy allocation mechanism is analyzed in the proposed model, and the corresponding reliability evaluation result is obtained under different terminal energy requirements. The approach is verified on the example of a dual hydraulic actuation system (DHAS), in which the stochastic model based on the generalized stochastic Petri nets (GSPNs) is established and combined with the power transfer capability via universal generating function (UGF). Though changing flow rate to face the degradation rate of hydraulic pump, the reliability assessment of DHAS based on the proposed reliability model is effective and accurate.

Keywords: reliability modeling, power transfer efficiency, multi-state performance, dual hydraulic actuation system, generalized stochastic Petri nets, universal generating function.

Układy przesyłu energii (power transfer systems, PTS) charakteryzują się szczególnymi właściwościami niezawodnościowymi, w tym wielostanowością i zależnością między błędami. W związku z tym, tradycyjne metody modelowania niezawodności, które sprawdzają się w przypadku systemów dwustanowych, nie pozwalają na dokładną ocenę niezawodności PTS. W przedstawionej pracy zaproponowano nowatorski model niezawodności systemu wielostanowego, który do oceny niezawodności PTS wykorzystuje dane o wydajności przesyłu energii (PTE). Model ten wiąże niezawodność zarówno z zapotrzebowaniem na energię końcową jak i zdolnością przesyłową PTS. Rozważano model wielostanowy opisujący proces degradacji komponentów systemu w oparciu o PTE. W proponowanym modelu analizowano korelacje między uszkodzeniami w świetle struktury systemu i mechanizmu alokacji energii, a niezawodność oceniano dla różnych stopni zapotrzebowania na energię końcową. Podejście to zweryfikowano na przykładzie podwójnego układu hydrauliki siłowej (DHAS), dla którego ustalono model stochastyczny oparty na uogólnionych stochastycznych sieciach Petriego (GSPN), który łączono ze zdolnością przesyłową za pomocą uniwersalnej funkcji tworzącej (UGF). Badania pompy hydraulicznej prowadzone dla różnych prędkości przepływu i różnych szybkości degradacji wykazały, iż ocena niezawodności DHAS na podstawie proponowanego modelu cechuje się skutecznością i trafnością.

Słowa kluczowe: modelowanie niezawodności, wydajność przesyłu energii, działanie systemu wielostanowego, podwójny układ hydrauliki siłowej, uogólnione stochastyczne sieci Petriego, uniwersalna funkcja tworząca.

1. Introduction

The systems in engineering field, in terms of their basic functions, can be divided into signal transfer system (STS), power transfer system (PTS), and mass transfer system (MTS). An STS, e.g. a sensor network, receives and transfers a series of analog/digital signals between terminals [9]. A PTS, e.g. a power transmission network, transforms and transmits energy between energy generators and consumers. An MTS transports mass between terminals. Due to the similar transmission characteristics derived from conservation law, an MTS can also be regarded as a special type of PTS [3, 7]. In this paper, only STS and PTS are considered. The correct implementation of functions requires that both STS and PTS have a complete transfer channel during the process of signal and energy transmitting. The impacts of random internal and external stresses acting on STS and PTS result in stochastic

behaviors of transmission function. Hence, the concept of reliability is adopted to describe STS and PTS's capability to fulfill their transmission function under stated conditions for a specific period of time [24]. However, there are big differences between reliability characteristics existing in STS and PTS. Firstly, an STS is a binary-state system, which means that the signal transmission is either "correct" or "incorrect". Therefore, "correct" or "incorrect" becomes a criterion to assess whether an STS fulfills its function or not. However, it is difficult to accurately assess a PTS's transmission quality based on "correct" and "incorrect", because the system exists obvious degradation states, viz. multi-state properties during power transmission process [5]. For example, the wear process of hydraulic pump results in multiple pressure and flow output probabilities. Hence, whether a hydraulic pump fulfills its function depends not only on its states, but also on

the terminal's energy requirements. Furthermore, an STS is generally a weak fault-coupling system, which means that a failed component in STS has small probability to influence other components, thus resulting in the component and/or system loss of function. The situation is completely different for a PTS, where a failed unit will change the energy distribution which may result in overload on other units, and ultimately these overloaded units will fail. For example, the hydraulic unit's sticking or jamming electro-hydrostatic actuator(EHA) on an aircraft may reduce hydraulic component's energy transmission efficiency, which will increase its forward motor's load, causing portion of the energy entering into the motor to be transformed to heat, which increases the probability of the motor failure [33, 35].

As discussed above, the different characteristics between STS and PTS raise challenges to assess and model the reliability uniformly. The traditional reliability model and assessment is established and conducted based on fault data with statistical theory [37]. This method can provide the probability density function based on the historical fault data and is suitable for STS' reliability assessment. Due to the lack of considering the fault behavior process, this reliability model cannot accurately describe the fault coupling among the components in PTS, and it also fails to assess the impact of multiple states on terminal's demands. In order to describe fault coupling relationship, researchers have developed numerous fault correlation models, e.g. copula models [14]. However, since these models describe the probability correlation among multiple faults based on data statistics, in the case of insufficient statistical data these models cannot reflect the probability characteristics of the faults. In order to build an accurate model of component's failure behavior in PTS, the physics of failure (PoF) method [31] is a good alternative. The PoF methods have been used quite successfully in modeling mechanical, civil, and aerospace structures. Reliability models based on failure physics can effectively capture failure processes, like fatigue, creep, wear, plastic deformation and instability. Peng et al. [22] applied PoF model to calculate the reliability of a micro-motor and determined the optimal maintenance strategy. Subsequently, it is found that the transfer of power along PTS will also affect its performance.

As a typical case of multi-state PTS, aircraft actuation system has distinct component degradation process and multiple power transfer states. Generally, aircraft actuation system with similar redundancy consists of three cross-linking units, viz. three independent hydraulic power sources, dissimilar redundant flight control computers and multiple redundant hydraulic actuators [26]. The effect of redundancy on risk and reliability can be calculated by using fault tree analysis (FTA) and reliability block diagram (RBD), but they are not very suitable for dynamic systems [1]. The critical components in aircraft power and actuation system are designed to be highly reliable to ensure safety, since the internal degradation and external events can cause extreme damage [29]. The Markov process method is more feasible to model both internal technical failures and external events dynamically [6]. Cross linking in three independent redundant hydraulic actuation systems can increase the survive channel under failures, then the reliability model based on failure monitoring and failure handoff appears to evaluate the system reliability under multiple faults [34]. More reliable and safety technologies make the flight control system more complex with dissimilar redundancy and multi separate control surfaces, e.g. A380 and B787 [25], in which surfaces are driven by both hydraulic power and electrical power. Accordingly, the aircraft actuation system based on multiple power resources and heterogeneous driving system becomes complicated cyber-physical system, in which the power supply systems, control computers and the actuators are different and complex fault tolerant strategies are designed. Under these circumstances, even if there are multiple faults, the performance of the actuation system can remain normal or slightly degraded, which is a specific multi-state system (MSS). The research on MSS began in the 1970s [8]. In recent years, multi-state systems

have been widely studied to describe multiple states of performance or the degradation process of components and systems. Various approaches have been proposed to estimate the reliability of MSS [19], including universal generating function (UGF) technique [11], stochastic process approach [23], and Monte Carlo simulation technique [30]. X. Li. et.al [15] even consider the multi-phased characteristics in the multi-state reliability assessment of the spacecraft. The control surface requires fast, accurate and smooth movement according to the control command. A specific amount of power flow transmitted from the input to the output measures the reliability considering flight performance. The reliability evaluation based on stochastic-flow network is first presented by Lee S H [12] and developed by Lin [17]. Lin [16] presented multi-state reliability method where Markov process was used to calculate the probability of states. If the state transfer is considered by time interval, the Markov process can be described as a Poisson process. Since Markovian method cannot characterize stress induced failure, Malinowski [21] presented corresponding numerical algorithm. Ushakov [27] presented UGF to solve the NP-hard problem of multi-state methods by defining the universal generating operator (UGO). Levitin [13] and Lisnianski [18] extended UGF to z-transform and verified this method on the physical system.

Aiming at modeling the reliability characteristics of aircraft actuation system, this paper presents a power flow-based reliability model, in which the power can be adjusted by pilot command and the fault reflected power loss. The multiple combination among power supply, computer and actuator under fault needs multi-state method to model its internal fault and fault transfer in the system. Multiple states in actuation system is reflected by the combinations of components' power transfer efficiency (PTE) which can be figured out by PoF analysis [10]. As an intuitive and effective method to analyze the dynamic processes of multi-elements degradation interior state, general stochastic Petri nets (GSPNs) [32] are adopted in this paper to model the functional states and degradation states of each component. In order to avoid solving massive differential equations, this paper adopts the UGF technique to calculate the system probability through algebraic calculus on the probability of component [28]. Through discretizing the continuous random variables and defining their probability distributions, a UGO can be obtained, then the availability can be calculated based on the UGF model [13, 18]. So, the multi-state reliability model via UGF is quite suitable for the case we studied.

The rest of this paper is presented as follows. In section 2, the reliability model based on PTE is formulated and the corresponding solution algorithm is introduced. With the UGF method, this paper calculates the probability of inner state of PTS. In Section 3, the case study of DHAS' reliability, which is a redundant actuation system composed of dual hydraulic source/hydraulic actuator and utilized in large aircraft [4], is computed and analyzed. In Section 4, conclusions are drawn.

2. Reliability assessment based on power transfer efficiency

Conventional reliability is defined as the probability that the component can perform its required function under stated conditions for a specified period of time [36]. Assuming that T is a random variable representing the failure time of a component, then the reliability is defined as the probability that the system will perform its expected function under the specified conditions of a given environment over a specified period of time t , namely:

$$R^c = P(T > t) = \int_t^{\infty} f(t) dt \quad (1)$$

where $f(t)$ is the failure probability density of the component, and $R^c(t)$ is the reliability of component at time t . This reliability model

is based on random failure mechanism under binary states, which is suitable for the reliability assessment of STS.

Practically, the performance of dynamic system is strongly related to its power supply and transmission that it is difficult to assess the system with only by “correct” or “incorrect”. For example, the hydraulic actuator of aircraft drives the control surface in a very wide frequency band, but the leakage of valve and cylinder will consume its power supply and degrade its performance. Therefore, whether a PTS fulfills its function depends not only on the states of its components, but also on the terminals’ energy demands. Assuming that W is the actual power supply provided for the PTS, and W_{th} is the minimum power requirement to guarantee its normal operation, then the reliability of PTS can be described as:

$$R^P = P(t | W \geq W_{th}). \quad (2)$$

Eq. (2) implies that the system power supply is sufficient to consumers’ requirements over the whole lifetime of the system. However, any component of PTS will dissipate the power during the operating process. It is difficult to keep enough power for the terminal output after experiencing power losses from multiple components. For instance, the aircraft actuation system could not drive the control surface according to the corresponding demand because of the internal and external leakage of system. In this situation, it is necessary to build the reliability model based on power supply and power transfer. This kind of reliability model can describe the failure process of PTS with the time increasing and the power being consumed.

Example 1: For a specific aircraft aileron control (shown in Fig. 1), its dynamic design processes are shown as follows in order to meet the actual requirements during each phase of flight profile. Suppose the control signal of aileron actuator is $x = x_0 \cdot \sin \omega t$, in which x_0 is the stroke of cylinder and ω is the frequency of actuator. According to the rated requirement, the maximum motion speed of actuator is $\dot{x}_{max} = 0.0838m/s$ and the minimum output force ensuring the normal movement of surface is $F=7500N$, then the reliability of aileron actuator can be described as:

$$R^P(t) = P(t | W \geq F \cdot \dot{x}_{max}) = P(t | W \geq 628.5 W). \quad (3)$$

where W is the actual power transferred by the actuation system to drive the aileron and $W_{th} = F \cdot \dot{x}_{max} = 628.5W$ is the minimal allowed power that can drive the surface under normal operational condition.

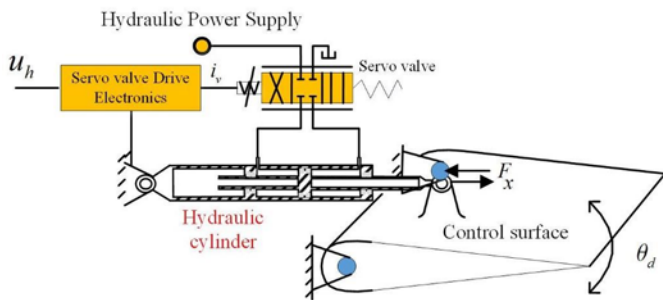


Fig. 1. The movement of aircraft aileron control

2.1. Assumptions and the general model

The reliability model of a PTS is developed based on the following assumptions:

- A PTS consists of n power transfer units (PTUs), in which the input power, the output power and the dissipated power of the $PTU_j (j=1,2,\dots,n)$ obey the power conservation law.
- Let η_j be the PTE of the $PTU_j (j=1,2,\dots,n)$. η_j decreases with the operational time increasing.
- The degradation of PTU_j can be described as a multi-state process with the occurrence and development of failure.
- The state of the $PTU_j (j=1,2,\dots,n)$ is statistically independent and the state duration obeys exponential distribution.
- c_j is the maximum allowed power capability under normal condition of the PTU_j , which is a constant.

As a fundamental physical component, the PTU and its performance determines PTS’ power transfer capability. In terms of power transmission process, $PTU_j (j=1,2,\dots,n)$ in PTS can be described as is shown in Fig. 2.

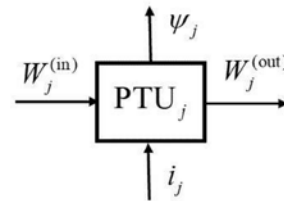


Fig. 2. A generic model based on power

For PTU_j , the input power $W_j^{(in)}$ entering PTU_j is transmitted to its downstream PTUs with the amount of $W_j^{(out)}$, while portion of power ψ_j is dissipated in the forms of heat and vibration. i_j represents the control signal of the unit according to the system requirement. Hence:

$$W_j^{(in)} = W_j^{(out)} + \psi_j \quad (4)$$

where $\eta_j = W_j^{(out)} / W_j^{(in)}$ defines the PTE of PTU_j

2.2. Stochastic power transmission model of PTU

Assuming that the initial power transmission capability of a PTU_j meets the PTS power requirements, the unit degrades with the operational time, as is shown in Fig. 3. The degradation process of PTU_j is divided into four states, viz. normal operation, light degradation, serious degradation and failure and the PTE η_j can be described as $\eta_j = [\eta_j^{(0)}, \eta_j^{(1)}, \eta_j^{(2)}, \eta_j^{(3)}]$. As a result, it is necessary to consider the multi-state process in power transmission model of PTU.

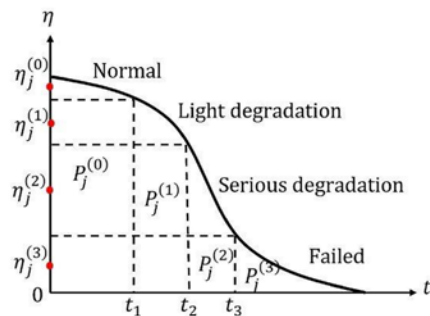


Fig. 3. Multi-state process of PTU_j

$PTU(\eta_j, A_j, P_j(t))$ is defined as a stochastic power transmission model for PTU_j , where $\eta_j = [\eta_j^{(0)}, \eta_j^{(1)}, \eta_j^{(2)}, \eta_j^{(3)}]^T$ denotes the PTE of PTU_j at normal state, light degradation state, serious degradation state and failed state, respectively. $P_j(t) = [P_j^{(0)}(t), P_j^{(1)}(t), P_j^{(2)}(t), P_j^{(3)}(t)]^T$ denotes the corresponding probabilities related to PTU_j at each state and A_j defines a stochastic process model relating PTU_j 's degradation with failure development.

In terms of its PTE, PTU_j 's operating states s_j are divided into four discrete intervals, $s_j \in \{s_0, s_1, s_2, s_3\}$, where different states denote that PTU_j has different power transmission capabilities, i.e.

$$W_j^{(out)} = \begin{cases} w_j^{(0)} = \eta_j^{(0)} W_j^{(in)} & s_j = s_0 \\ w_j^{(1)} = \eta_j^{(1)} W_j^{(in)} & s_j = s_1 \\ w_j^{(2)} = \eta_j^{(2)} W_j^{(in)} & s_j = s_2 \\ w_j^{(3)} = \eta_j^{(3)} W_j^{(in)} & s_j = s_3 \end{cases} \quad (5)$$

Example 2: A hydraulic pump's PTE decreases as its components experiencing wear and tear. Fig. 4 (a) illustrates the wear process of slippers inside a hydraulic pump. According to the Archard's model, the abrasion loss of slippers can be described as follows:

$$\frac{d\varphi_w}{dt} = k_w \frac{q_w}{A_w} \quad (6)$$

where φ_w is the abrasion loss, $d\varphi_w/dt$ is the wear rate, k_w is constantly related to the surface condition and lubrication within the friction pair, q_w is the load on the wear surface, and A_w is the contact area of the wear surface. The abrasion loss curve is illustrated in Fig. 4 (b). As the slippers wear over time, the volumetric efficiency (VE) of the pump decreases, and it leads to the reduction of the effective power of the output, as shown in Fig. 4 (c).

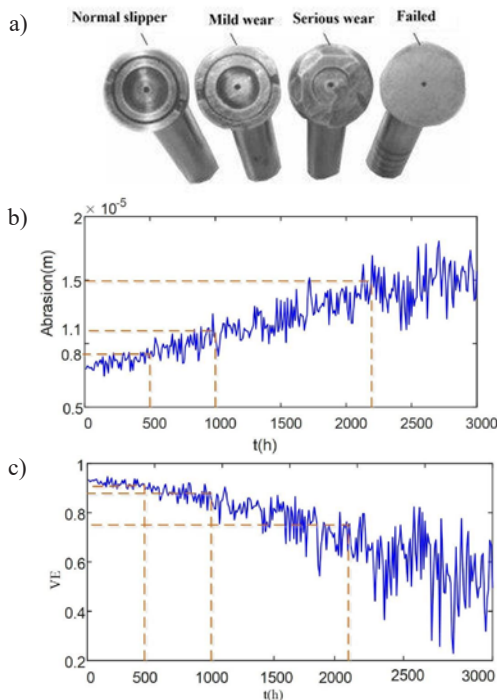


Fig. 4. Illustration of multi-state for hydraulic pump caused by wear; a) Wear process of slipper in pump, b) Abrasion loss of slippers, c) VE of the pump

According to Fig. 4 (b), during the time interval $[0, 500h)$, the slippers' abrasion is less than $0.8 \times 10^{-5} m$. The corresponding VE of the pump is in the interval of $[0.92, 0.95]$, and can be regarded as a normal state of the hydraulic pump. During the time interval $[500h, 1000h)$, the abrasion loss of slippers is in the interval of $[0.8 \times 10^{-5} m, 1.1 \times 10^{-5} m)$ and the VE of the pump is $[0.9, 0.92]$. This state is defined as a light degradation state. As the pump continue to be used, in the time interval $[1000h, 2000h)$ the slippers' abrasion is in the interval of $[1.1 \times 10^{-5} m, 1.5 \times 10^{-5} m)$ and the corresponding VE of the pump is $[0.75, 0.9]$. Fig. 4 (c), describes a serious degradation state of the hydraulic pump. After 2000 hours, the slippers' abrasion becomes serious and the corresponding VE is less than 0.75, which cannot meet the demand of the downstream PTUs. We define this state as a failed state for the hydraulic pump.

In order to characterize the development of failure, GSPN model is used to establish the internal state transition process of PTU_j . Defining A_j as the state transition matrix, the probabilities of PTU_j , $P_j(t) = [P_j^{(0)}(t), P_j^{(1)}(t), P_j^{(2)}(t), P_j^{(3)}(t)]^T$ can be obtained by:

$$P_j(t+1) = A_j \cdot P_j(t) \quad (7)$$

$s_j = \{s_j^{(k)} | (P_j^{(k)}(t), \eta_j^{(k)}), k = 0, 1, 2, 3\}$ describes the power transfer state of PTU_j at time t . UGF method is applied to simplify the calculation of the PTU state and its corresponding probability. For PTU_j , the PTE-based model, $PTU(\eta_j, A_j, P_j(t))$, can be written as:

$$PTU(\eta_j, A_j, P_j(t)) = P_j^{(0)}(t)z^{\eta_j^{(0)}} + P_j^{(1)}(t)z^{\eta_j^{(1)}} + P_j^{(2)}(t)z^{\eta_j^{(2)}} + P_j^{(3)}(t)z^{\eta_j^{(3)}} \quad (8)$$

2.3. Reliability model based on power transfer efficiency

For a PTS with n PTU s, as is shown in Fig. 5, the input power $W_{sys}^{(in)}$ is transmitted to terminal users in channels composed of individual PTU s in the form of parallel or serial layout. The PTE of a PTS also depends on multiple states that $s_{sys}^{(i)} = (P_{sys}^{(i)}(t), \eta_{sys}^{(i)})$, $i = 0, 1, 2, \dots, 4^n - 1$ represents the i^{th} state of PTS at time t , which means that the PTS has PTE $\eta_{sys}^{(i)}$ with the probability of $P_{sys}^{(i)}(t)$.

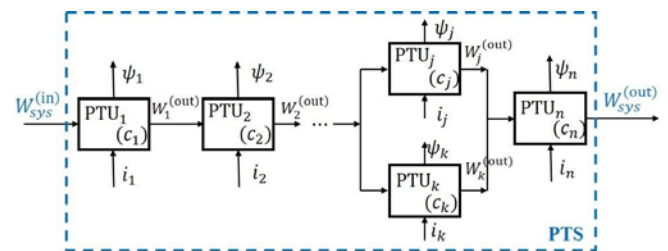


Fig. 5. Illustration of PTS structure

Given PTU 's PTE-based models, $PTU(\eta_j, A_j, P_j(t))$, $j = 1, 2, \dots, n$, the PTS' model can be described as:

$$PTS(\eta_{sys}, P_{sys}(t)) = PTS(\Theta(\eta_1, \eta_2, \dots, \eta_n), g(P_1(t), P_2(t), \dots, P_n(t))) \quad (9)$$

where the structural functions Θ and g describe mathematical relationships of PTE and corresponding probabilities of PTS and its com-

ponents. The forms of Θ and g are determined by layout structure among PTUs. In engineering application, there are two typical connecting structures among PTUs, i.e. series layout and parallel layout.

2.3.1. PTE-base reliability model for series system

For a structure serialized by m PTUs, as shown in Fig. 6, the model of PTS can be described by Eq. (10).

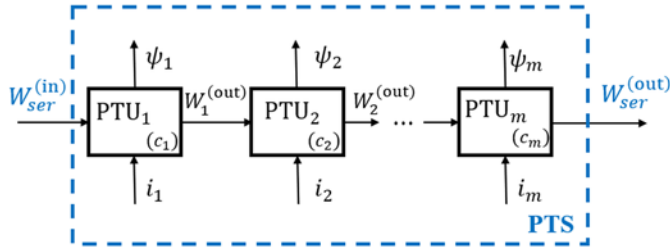


Fig. 6. Illustration of a structure serialized by m PTUs

$$\begin{aligned}
 \text{PTS}(\eta_{ser}, P_{ser}(t)) &= \text{PTU}(\eta_1, A_1, P_1(t)) \otimes \dots \otimes \text{PTU}(\eta_m, A_m, P_m(t)) \\
 &= \sum_{i_1=1}^4 \sum_{i_2=1}^4 \dots \sum_{i_m=1}^4 \left(\prod_{j=1}^m \prod_{k=1}^4 P_j^{(i_k)}(t) \right) z^{\prod_{j=1}^m \prod_{k=1}^4 \eta_j^{(i_k)}}
 \end{aligned} \tag{10}$$

The i^{th} state in $s_{ser}^{(i)} = (P_{ser}^{(i)}(t), \eta_{ser}^{(i)})$ is $s_{ser}^{(i)} \in (s_1^{i_1}, s_2^{i_2}, \dots, s_m^{i_m})$ and its PTE can be calculated by:

$$\begin{aligned}
 W_1^{(out)} &= W_{ser}^{(in)} \cdot \eta_1^{i_1} \\
 W_2^{(out)} &= W_1^{(out)} \cdot \eta_2^{i_2} \\
 &\dots \\
 W_{ser}^{(out)} &= W_{m-1}^{(out)} \cdot \eta_m^{i_m}
 \end{aligned} \tag{11}$$

The PTE for the serial system shown in Fig. 6 is $\eta_{ser}^{(i)} = W_{ser}^{(out)} / W_{ser}^{(in)} = \eta_1^{(i_1)} \cdot \eta_2^{(i_2)} \dots \eta_m^{(i_m)}$ and the corresponding probability is $P_{sys}^{(i)}(t) = P_1^{(i_1)}(t) \cdot P_2^{(i_2)}(t) \dots P_m^{(i_m)}(t)$.

Example 3: Assume that two PTUs are serially connected. The operator \otimes is defined to describe the serial operation and the i^{th} state probability of the PTS and its corresponding PTE is given by Eq. (12), with four states in each PTU.

$$\begin{aligned}
 \text{PTS}(\eta_{ser}, P_{ser}(t)) &= \text{PTU}(\eta_1, A_1, P_1(t)) \otimes \text{PTU}(\eta_2, A_2, P_2(t)) \\
 &= P_1^{(0)}(t)P_2^{(0)}(t)z^{\eta_1^{(0)}\eta_2^{(0)}} + P_1^{(0)}(t)P_2^{(1)}(t)z^{\eta_1^{(0)}\eta_2^{(1)}} + P_1^{(0)}(t)P_2^{(2)}(t)z^{\eta_1^{(0)}\eta_2^{(2)}} + P_1^{(0)}(t)P_2^{(3)}(t)z^{\eta_1^{(0)}\eta_2^{(3)}} \\
 &\quad + P_1^{(1)}(t)P_2^{(0)}(t)z^{\eta_1^{(1)}\eta_2^{(0)}} + P_1^{(1)}(t)P_2^{(1)}(t)z^{\eta_1^{(1)}\eta_2^{(1)}} + P_1^{(1)}(t)P_2^{(2)}(t)z^{\eta_1^{(1)}\eta_2^{(2)}} + P_1^{(1)}(t)P_2^{(3)}(t)z^{\eta_1^{(1)}\eta_2^{(3)}} \\
 &\quad + P_1^{(2)}(t)P_2^{(0)}(t)z^{\eta_1^{(2)}\eta_2^{(0)}} + P_1^{(2)}(t)P_2^{(1)}(t)z^{\eta_1^{(2)}\eta_2^{(1)}} + P_1^{(2)}(t)P_2^{(2)}(t)z^{\eta_1^{(2)}\eta_2^{(2)}} + P_1^{(2)}(t)P_2^{(3)}(t)z^{\eta_1^{(2)}\eta_2^{(3)}} \\
 &\quad + P_1^{(3)}(t)P_2^{(0)}(t)z^{\eta_1^{(3)}\eta_2^{(0)}} + P_1^{(3)}(t)P_2^{(1)}(t)z^{\eta_1^{(3)}\eta_2^{(1)}} + P_1^{(3)}(t)P_2^{(2)}(t)z^{\eta_1^{(3)}\eta_2^{(2)}} + P_1^{(3)}(t)P_2^{(3)}(t)z^{\eta_1^{(3)}\eta_2^{(3)}}
 \end{aligned} \tag{12}$$

2.3.2. PTE-based reliability model for parallel system

Fig. 7 shows a parallel structure of a PTS, in which PTUs transfer the input power to terminal customers. Assume that the input of j^{th} PTU is $c_j \cdot W_{par}^{(in)} / \sum_{i=1}^m c_i$ where c_j denotes the capacity of PTU j , which indicates the ability to cope with the input power. The capacity of each PTU determines the power allocation among components.

The parallel structure in a PTS' model can be described as:

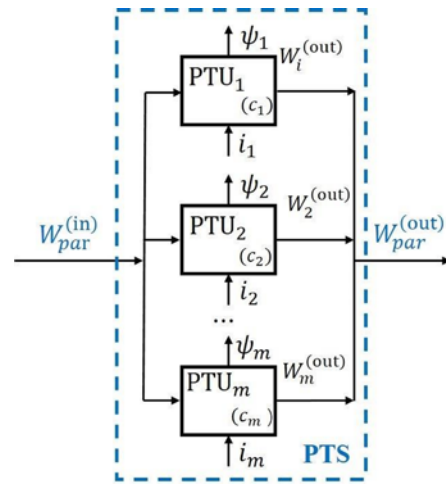


Fig. 7. Illustration of a parallel structure by m PTUs

$$\begin{aligned}
 \text{PTS}(\eta_{par}, P_{par}(t)) &= \text{PTU}(\eta_1, A_1, P_1(t)) \oplus \dots \oplus \text{PTU}(\eta_m, A_m, P_m(t)) \\
 &= \sum_{i_1=1}^4 \sum_{i_2=1}^4 \dots \sum_{i_m=1}^4 \left(\prod_{j=1}^m \prod_{k=1}^4 P_j^{(i_k)}(t) \right) z^{\frac{c_1\eta_1^{(i_1)} + c_2\eta_2^{(i_2)} + \dots + c_m\eta_m^{(i_m)}}{\sum_{i=1}^m c_i} \sum_{j=1}^m \sum_{k=1}^4 \eta_j^{(i_k)}}
 \end{aligned} \tag{13}$$

The i^{th} state in PTS $s_{par}^{(i)} = (P_{par}^{(i)}(t), \eta_{par}^{(i)})$ is $s_{par}^{(i)} \in (s_1^{i_1}, s_2^{i_2}, \dots, s_m^{i_m})$ and its PTE can be obtained by:

$$\begin{aligned}
 W_1^{(in)} &= W_{par}^{(in)} \cdot \frac{c_1}{\sum_{i=1}^m c_i}, W_1^{(out)} = \eta_1^{(i_1)} \cdot W_1^{(in)} \\
 W_2^{(in)} &= W_{par}^{(in)} \cdot \frac{c_2}{\sum_{i=1}^m c_i}, W_2^{(out)} = \eta_2^{(i_2)} \cdot W_2^{(in)} \\
 &\dots \\
 W_m^{(in)} &= W_{par}^{(in)} \cdot \frac{c_m}{\sum_{i=1}^m c_i}, W_m^{(out)} = \eta_m^{(i_m)} \cdot W_m^{(in)}
 \end{aligned} \tag{14}$$

Then,

$$W_{par}^{(out)} = W_1^{(out)} + W_2^{(out)} + \dots + W_m^{(out)} = W_{par}^{(in)} \left(\frac{c_1}{\sum_{i=1}^m c_i} \eta_1^{(i_1)} + \frac{c_2}{\sum_{i=1}^m c_i} \eta_2^{(i_2)} + \dots + \frac{c_m}{\sum_{i=1}^m c_i} \eta_m^{(i_m)} \right)$$

The PTE of the i^{th} state for the parallel structure, as is shown in Fig. 7, is $\eta_{par}^{(i)} = \frac{W_{par}^{(out)}}{W_{par}^{(in)}} = \frac{1}{\sum_{i=1}^m c_i} (c_1\eta_1^{(i_1)} + c_2\eta_2^{(i_2)} + \dots + c_m\eta_m^{(i_m)})$ and

the corresponding probability can be calculated as $P_{par}^{(i)}(t) = P_1^{(i_1)}(t) \cdot P_2^{(i_2)}(t) \dots P_m^{(i_m)}(t)$.

Example 4: Two PTUs are connected by parallel structure. The operator \oplus is defined to describe the parallel operation. The PTS' i^{th} state probability and its corresponding PTE can be obtained by:

$$\begin{aligned}
 \text{PTS}(\eta_{par}, \mathbf{P}_{par}(t)) &= \text{PTU}(\eta_1, \mathbf{A}_1, \mathbf{P}_1(t)) \oplus \text{PTU}(\eta_2, \mathbf{A}_2, \mathbf{P}_2(t)) \\
 &= P_1^{(0)}(t)P_2^{(0)}(t)z^{\frac{c_1\eta_1^{(0)}+c_2\eta_2^{(0)}}{c_1+c_2}} + P_1^{(0)}(t)P_2^{(1)}(t)z^{\frac{c_1\eta_1^{(0)}+c_2\eta_2^{(1)}}{c_1+c_2}} + P_1^{(0)}(t)P_2^{(2)}(t)z^{\frac{c_1\eta_1^{(0)}+c_2\eta_2^{(2)}}{c_1+c_2}} + P_1^{(0)}(t)P_2^{(3)}(t)z^{\frac{c_1\eta_1^{(0)}+c_2\eta_2^{(3)}}{c_1+c_2}} \\
 &\quad + P_1^{(1)}(t)P_2^{(0)}(t)z^{\frac{c_1\eta_1^{(1)}+c_2\eta_2^{(0)}}{c_1+c_2}} + P_1^{(1)}(t)P_2^{(1)}(t)z^{\frac{c_1\eta_1^{(1)}+c_2\eta_2^{(1)}}{c_1+c_2}} + P_1^{(1)}(t)P_2^{(2)}(t)z^{\frac{c_1\eta_1^{(1)}+c_2\eta_2^{(2)}}{c_1+c_2}} + P_1^{(1)}(t)P_2^{(3)}(t)z^{\frac{c_1\eta_1^{(1)}+c_2\eta_2^{(3)}}{c_1+c_2}} \\
 &\quad + P_1^{(2)}(t)P_2^{(0)}(t)z^{\frac{c_1\eta_1^{(2)}+c_2\eta_2^{(0)}}{c_1+c_2}} + P_1^{(2)}(t)P_2^{(1)}(t)z^{\frac{c_1\eta_1^{(2)}+c_2\eta_2^{(1)}}{c_1+c_2}} + P_1^{(2)}(t)P_2^{(2)}(t)z^{\frac{c_1\eta_1^{(2)}+c_2\eta_2^{(2)}}{c_1+c_2}} + P_1^{(2)}(t)P_2^{(3)}(t)z^{\frac{c_1\eta_1^{(2)}+c_2\eta_2^{(3)}}{c_1+c_2}} \\
 &\quad + P_1^{(3)}(t)P_2^{(0)}(t)z^{\frac{c_1\eta_1^{(3)}+c_2\eta_2^{(0)}}{c_1+c_2}} + P_1^{(3)}(t)P_2^{(1)}(t)z^{\frac{c_1\eta_1^{(3)}+c_2\eta_2^{(1)}}{c_1+c_2}} + P_1^{(3)}(t)P_2^{(2)}(t)z^{\frac{c_1\eta_1^{(3)}+c_2\eta_2^{(2)}}{c_1+c_2}} + P_1^{(3)}(t)P_2^{(3)}(t)z^{\frac{c_1\eta_1^{(3)}+c_2\eta_2^{(3)}}{c_1+c_2}}
 \end{aligned} \tag{15}$$

The effective implementation of the function for the system depends on whether the input energy can meet the energy requirements of the drive system. Through the expression of the PTE-based model mentioned above, the reliability that the system can meet the energy demand $W^{(d)}$ can be introduced as:

$$R^P(t | W_{sys}^{(out)} \geq W^{(d)}) = \sum_{i=1}^m \left\{ p_{sys}^{(i)}(t) \cdot \mathbf{1}(\eta_{sys}^{(i)} \cdot W_{sys}^{(in)} - W^{(d)} \geq 0) \right\} \tag{16}$$

$$\text{where } \mathbf{1}(\eta_{sys}^{(i)} \cdot W_{sys}^{(in)} - W^{(d)} \geq 0) = \begin{cases} 1, & \eta_{sys}^{(i)} \cdot W_{sys}^{(in)} - W^{(d)} \geq 0 \\ 0, & \eta_{sys}^{(i)} \cdot W_{sys}^{(in)} - W^{(d)} < 0 \end{cases}$$

Fig. 8 shows the flow chart of the reliability assessment method based on PTE. Firstly, the degradation analysis based on PTE model with multiple states is carried out and the corresponding probability of the states can be calculated by GSPN. Then, UGF is used to calculate the probability of PTU states and the system with u-function. Finally, the reliability assessment can be obtained based on the power threshold boundary.

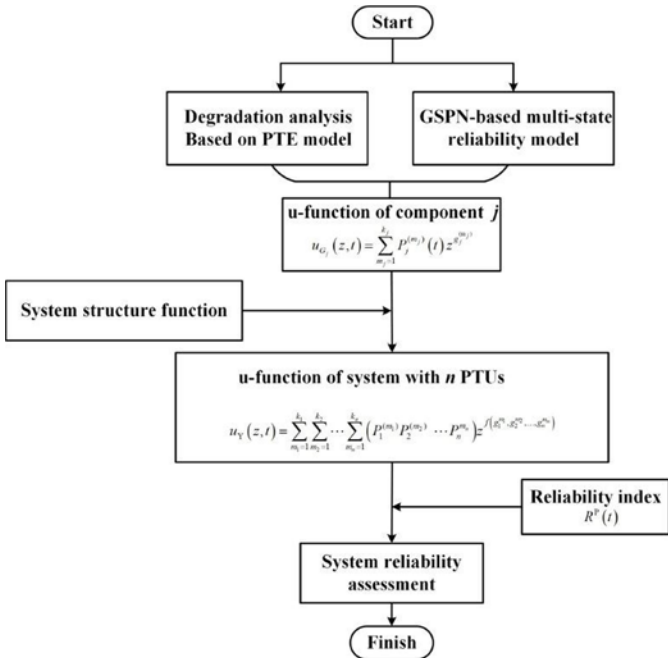


Fig. 8. Flow chart of the reliability assessment of PTS based on PTE

3. Case study of dual hydraulic actuation system

3.1. System description

Dual hydraulic actuation system (DHAS) is a typical PTS which drives the control surfaces of civil aircraft, shown in Fig. 9, in which

the hydraulic pump transfers the energy from engine through accessory gearbox, servo valve controls the flow of cylinder according to command and the cylinder drives the control surface with high pressure oil. Components in DHAS can be regarded as PTUs with power dissipation. In order to keep high reliability, DHAS adopts dual redundant hydraulic power supply systems and actuators.

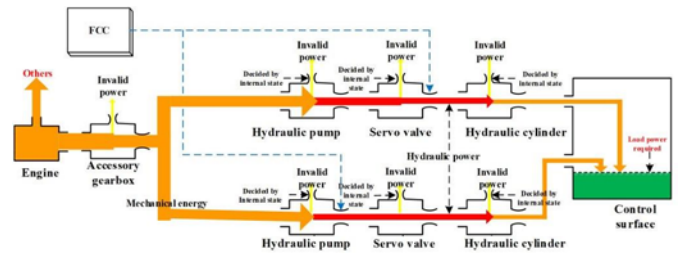


Fig. 9. Structure diagram and power transmission of DHAS

Hydraulic pump transfers a portion of aircraft engine power to high pressure hydraulic power supply, which drives the control surface according to the DHAS control command. Whether the DHAS can provide enough power to drive the control surface with very quick response depends on components' performance degradation and its external destruction. According to Section 2.3, a PTE-based model for DHAS can be built as is shown in Fig. 10.

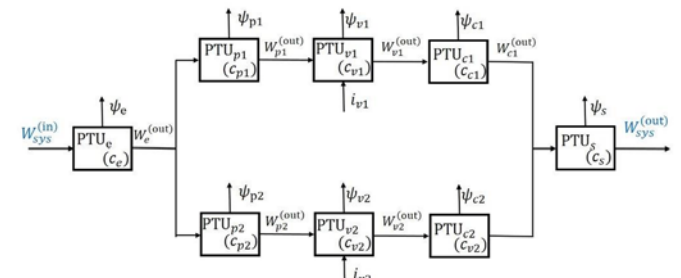


Fig. 10. PTE-based model of each PTU in DHAS

In Fig. 10, the output power of aircraft engine $W_{sys}^{(in)}$ is firstly transferred into accessory gearbox $\text{PTU}(\eta_G, \mathbf{P}_G(t))$, then the output power of accessory gearbox $W_G^{(out)}$ is inputted to DHAS channels. In DHAS channel, the primary hydraulic pump $\text{PTU}(\eta_{p1}, \mathbf{A}_{p1}, \mathbf{P}_{p1}(t))$ and the secondary hydraulic pump $\text{PTU}(\eta_{p2}, \mathbf{A}_{p2}, \mathbf{P}_{p2}(t))$ receive the power and transfer the power into pressurized hydraulic oil. The servo valves $\text{PTU}(\eta_{v1}, \mathbf{A}_{v1}, \mathbf{P}_{v1}(t))$ and $\text{PTU}(\eta_{v2}, \mathbf{A}_{v2}, \mathbf{P}_{v2}(t))$ receive control signals from flight control computers and drive the corresponding hydraulic cylinder, $\text{PTU}(\eta_{c1}, \mathbf{A}_{c1}, \mathbf{P}_{c1}(t))$ or $\text{PTU}(\eta_{c2}, \mathbf{A}_{c2}, \mathbf{P}_{c2}(t))$.

The dual hydraulic cylinders integrate to drive the control surface $(\eta_{sur}, \mathbf{P}_{sur}(t))$. The output power $W_{sys}^{(out)}$ works as the speed and out-

put force on control surfaces. Supposing that the $W_{sur}^{(d)}$ is the minimum required power of control surface under normal performance, the reliability of DHAS can be described as:

$$R_{DHAS}^P(t) = P(t | W_{sys}^{(out)} \geq W_{sur}^{(d)}) \quad (17)$$

For each channel of the DHAS, according to Eq. (10), the PTE-based model can be written as:

$$\begin{aligned} DHAS_1(\eta_{DHAS_1}, P_{DHAS_1}(t)) &= PTU(\eta_{P_1}, A_{P_1}, P_{P_1}(t)) \otimes PTU(\eta_{V_1}, A_{V_1}, P_{V_1}(t)) \otimes PTU(\eta_{C_1}, A_{C_1}, P_{C_1}(t)) \\ DHAS_2(\eta_{DHAS_2}, P_{DHAS_2}(t)) &= PTU(\eta_{P_2}, A_{P_2}, P_{P_2}(t)) \otimes PTU(\eta_{V_2}, A_{V_2}, P_{V_2}(t)) \otimes PTU(\eta_{C_2}, A_{C_2}, P_{C_2}(t)) \end{aligned} \quad (18)$$

Then, the PTE-based model for the whole DHAS can be written as:

$$\begin{aligned} DHAS(\eta_{DHAS}, P_{DHAS}(t)) &= PTU(\eta_G, P_G(t)) \otimes \\ & (DHAS_1(\eta_{DHAS_1}, P_{DHAS_1}(t)) \oplus DHAS_2(\eta_{DHAS_2}, P_{DHAS_2}(t))) \otimes (\eta_{sur}, P_{sur}(t)) \end{aligned} \quad (19)$$

Here the DHAS of Airbus380 is selected as a case study in real flight profile. The worst scenario is considered, whereby a failure of the control surface will result in the loss of the aircraft, and the demand is that such event must have a probability of less than 1×10^{-9} per flight hour. The failure rates assumed for each type of component are listed in Table 1 [2].

Table 1. Failure rates for each component

Component	Mechanical	Controller	Power supply
Failure rate λ	$2.2 \times 10^{-6} / h$	$8.6 \times 10^{-5} / h$	$5.4 \times 10^{-5} / h$

3.2. PTE-based reliability model of individual PTU in DHAS

In Fig. 10, the main components in DHAS include hydraulic pump, servo valves and hydraulic cylinders. The PTE-based reliability model of above PTU is built as follows.

3.2.1. Hydraulic pump

The structure of an aircraft axial piston pump is shown in Fig. 11. A conventional piston pump provides the pressurized oil through the pistons reciprocating within their bores, in which the displaced volume from the pump is controlled by the inclination angle of the

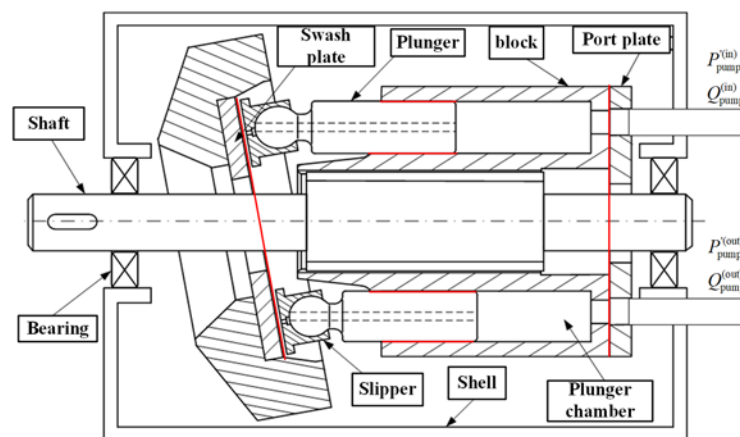


Fig. 11. Operating principle and components of a piston hydraulic pump

hanger. The failure behavior of the pump is a progressive failure process caused by wear [2].

The power output of hydraulic pump, $W_p^{(out)}$, is influenced by two different random effects:

- 1) the input power comes from the engine accessory gearbox $W_G^{(in)}$.
- 2) the efficiency of hydraulic pump, $\eta_p = \eta_p^{(M)} \eta_p^{(V)}$ wherein, $\eta_p^{(M)}$ denotes the mechanical efficiency and $\eta_p^{(V)}$ denotes the volumetric efficiency. Therefore:

$$W_p^{(out)} = \eta_p^{(M)} \eta_p^{(V)} \cdot W_p^{(in)} \quad (20)$$

For the volumetric efficiency of the pump:

$$\eta_p^{(V)} = 1 - \frac{\Delta Q_p}{n_p V} \quad (21)$$

wherein, ΔQ_p is the internal leakage flow of pump and V is theoretical displacement of pump.

The wear of the friction pairs in a hydraulic pump, e.g., the wear of the plunger-plunger cavity on rotor, will increase the clearance of the friction pairs which enlarges the oil leakage ΔQ_p . $\eta_p^{(V)}$ will then decrease accordingly, as shown in Fig. 4.

The mechanical efficiency, $\eta_p^{(M)}$, is determined by the conditions of mechanical-linkage system between the hydraulic pump and driving devices. This paper ignores the mechanical efficiency and only discusses the impacts of the volumetric efficiency.

According to the value of $\eta_p^{(V)}$ the states of pump are divided into four discrete cases, i.e.:

$$s_p = \begin{cases} s_{p0} & \eta_p^{(0)} \in [0.92, 1] \\ s_{p1} & \eta_p^{(1)} \in [0.9, 0.92] \\ s_{p2} & \eta_p^{(2)} \in [0.75, 0.9] \\ s_{p3} & \eta_p^{(3)} \in [0, 0.75] \end{cases} \quad (22)$$

When $\eta_p \geq 0.92$, the pump operates very well, and s_{p0} is named as the normal state of the hydraulic pump. With the development of internal wear, the value of η_p decreases into the interval of $[0.9, 0.92]$. In this case, the pump operates well despite the small amount of wear, so s_{p1} is named as the light degradation state. The value of η_p decreases into the interval of $[0.75, 0.9]$ with continuous accumulation of wear, the performance of hydraulic pump degrades obviously, thus s_{p2} is named as serious degradation state. Once $\eta_p < 0.75$, the pump will be regarded as failed. Median value of each interval is used as the indicator and we get $\eta_p = [\eta_p^{(0)}, \eta_p^{(1)}, \eta_p^{(2)}, \eta_p^{(3)}]^T = [0.96, 0.91, 0.825, 0.375]^T$.

In order to get the probabilities corresponding to $s_p = [s_{p0}, s_{p1}, s_{p2}, s_{p3}]$, a GSPN-based state transition model is established as shown in Fig. 12.

According to the GSPN model, at time 0, pump starts from the normally functioning state, $\#(PUMP.up)=1$. After a period of time t_{p1} , pump may directly fail with the probability $P(t_{p13})$, which is described by a token being transmitted directly from PUMP.up to PUMP.dn. Alternatively, the pump can degrade through a gradual failure mode with probability $P(t_{p11})$, and

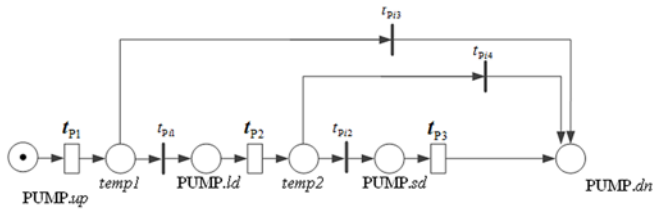


Fig. 12. The GSPN model of hydraulic pump performance degradation process

then pump enters the light degradation state, i.e. #(PUMP.ld)=1. Here, $P(t_{p_{i3}}) + P(t_{p_{i1}}) = 1$. The transfer rate of the timed transition t_{p1} is λ_{p1} , so that $P(t_{p_{i3}})\lambda_{p1}$ describes the failure rate of pump from normal operating state to complete failure, and $P(t_{p_{i1}})\lambda_{p1}$ describes the failure rate of pump from normal operating state to light degradation state. As operational time increasing, pump may suffer additional performance degradation leading directly to complete failure, i.e., entering the down state (PUMP.dn), or firstly reaching to the serious degradation state (PUMP.sd) and the token is correspondingly transferred with probability of $P(t_{p_{i4}})$. Here, $P(t_{p_{i4}}) + P(t_{p_{i2}}) = 1$ and $P(t_{p_{i1}}) + P(t_{p_{i3}}) = 1$. The $temp_i (i = 1, 2)$ represents temporary states in the GSPN modeling of the hydraulic pump performance degradation process. Given the initial work condition, the steady state probabilities of the pump states can be obtained by simulation. This part is adapted from the original work proposed by authors previously [29].

GSPN-based model of hydraulic pump only describes its degradation process. To obtain $\mathbf{P}_p(t)$, the Markov process model which equivalent to GSPN model is illustrated in Fig. 13.

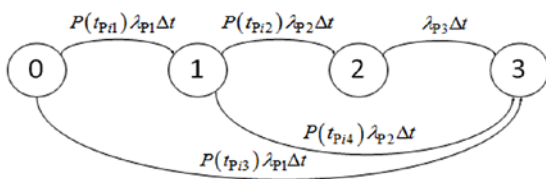


Fig. 13. The mechanical degradation states of hydraulic pump

The corresponding relationship between states of GSPN model and Markov model is illustrated in Table 2.

Table 2. The corresponding relationship between states of GSPN model and Markov model

No.	States in Markov Model	States in GSPN model	Description
1	'0'	#(PUMP.up)=1	The normally state of pump
2	'1'	#(PUMP.ld)=1	The light degradation state of pump
3	'2'	#(PUMP.sd)=1	The serious degradation state of pump
4	'3'	#(PUMP.dn)=1	The failure state of pump

The state transition matrix of hydraulic pump, \mathbf{A}_p , can be written as:

$$A_p = \begin{bmatrix} -(P(t_{p_{i1}})\lambda_{p1} + P(t_{p_{i3}})\lambda_{p1}) & 0 & 0 & 0 \\ P(t_{p_{i1}})\lambda_{p1} & -(P(t_{p_{i2}})\lambda_{p2} + P(t_{p_{i4}})\lambda_{p2}) & 0 & 0 \\ 0 & P(t_{p_{i2}})\lambda_{p2} & -\lambda_{p3} & 0 \\ P(t_{p_{i3}})\lambda_{p1} & P(t_{p_{i4}})\lambda_{p2} & \lambda_{p3} & 0 \end{bmatrix} = \begin{bmatrix} a_{11} & 0 & 0 & 0 \\ a_{21} & a_{22} & 0 & 0 \\ 0 & a_{32} & a_{33} & 0 \\ a_{41} & a_{42} & a_{43} & 0 \end{bmatrix} \quad (23)$$

The probabilities that the hydraulic pump stays in $\mathbf{s}_p = [s_{p0}, s_{p1}, s_{p2}, s_{p3}]$ can be obtained according to Eq. (7) and the derivation is shown below:

$$\begin{aligned} P_p^{(0)}(t) &= e^{a_{11}t} \\ P_p^{(1)}(t) &= \frac{a_{21}}{a_{11} - a_{22}} (e^{a_{11}t} - e^{a_{22}t}) \\ P_p^{(2)}(t) &= \frac{a_{21}a_{32}}{(a_{11} - a_{22})(a_{11} - a_{33})} e^{a_{11}t} + \frac{a_{21}a_{32}}{(a_{22} - a_{11})(a_{22} - a_{33})} e^{a_{22}t} + \frac{a_{21}a_{32}}{(a_{33} - a_{11})(a_{33} - a_{22})} e^{a_{33}t} \\ P_p^{(3)}(t) &= \left[\frac{a_{41}}{a_{11}} + \frac{a_{21}a_{42}}{a_{11}a_{22}} - \frac{a_{21}a_{32}a_{43}}{a_{11}a_{22}a_{33}} \right] e^{a_{11}t} + \left[\frac{a_{41}}{a_{11}} + \frac{a_{21}a_{42}}{a_{11}(a_{11} - a_{22})} + \frac{a_{21}a_{32}a_{43}}{a_{11}(a_{11} - a_{22})(a_{11} - a_{33})} \right] e^{a_{11}t} \\ &+ \left[\frac{a_{21}a_{42}}{a_{22}(a_{22} - a_{11})} + \frac{a_{21}a_{32}a_{43}}{a_{22}(a_{22} - a_{11})(a_{22} - a_{33})} \right] e^{a_{22}t} + \frac{a_{21}a_{32}a_{43}}{a_{33}(a_{33} - a_{11})(a_{33} - a_{22})} e^{a_{33}t} \end{aligned} \quad (24)$$

The parameters of the hydraulic pump model of Fig. 13 are listed in Table 3 [29].

Table 3. Parameters of Pump model

Parameter	Value	Parameter	Value
$P(t_{p_{i1}})$	0.9	$P(t_{p_{i2}})$	0.3
$P(t_{p_{i3}})$	0.1	$P(t_{p_{i4}})$	0.7
λ_{p1}	$5.4 \times 10^{-5} / h$	λ_{p2}	$6.0 \times 10^{-5} / h$
λ_{p3}	$6.8 \times 10^{-5} / h$		

Then, the probabilities of the pump states can be obtained:

$$P_p(t) = \begin{bmatrix} P_p^{(0)}(t) \\ P_p^{(1)}(t) \\ P_p^{(2)}(t) \\ P_p^{(3)}(t) \end{bmatrix} = \begin{bmatrix} e^{-5.4 \times 10^{-5}t} \\ 8.1 \times (e^{-5.4 \times 10^{-5}t} - e^{-6.0 \times 10^{-5}t}) \\ 10.41e^{-5.4 \times 10^{-5}t} - 18.23e^{-6.0 \times 10^{-5}t} + 7.82e^{-6.8 \times 10^{-5}t} \\ 1 - 19.51e^{-5.4 \times 10^{-5}t} + 26.33e^{-6.0 \times 10^{-5}t} - 7.82e^{-6.8 \times 10^{-5}t} \end{bmatrix} \quad (25)$$

The probability curves of the pump states are illustrated in Fig. 14.

Therefore, for a hydraulic pump, the stochastic power transmission model, $PTU(\eta_p, \mathbf{A}_p, \mathbf{P}_p(t))$, can be written as:

$$\begin{aligned} PTU(\eta_p, \mathbf{A}_p, \mathbf{P}_p(t)) &= P_p^{(0)}(t)z^{\eta_p^{(0)}} + P_p^{(1)}(t)z^{\eta_p^{(1)}} + P_p^{(2)}(t)z^{\eta_p^{(2)}} + P_p^{(3)}(t)z^{\eta_p^{(3)}} \\ &= e^{-5.4 \times 10^{-5}t} z^{0.96} + 8.1 \times (e^{-5.4 \times 10^{-5}t} - e^{-6.0 \times 10^{-5}t}) z^{0.91} \\ &+ \left[10.41e^{-5.4 \times 10^{-5}t} - 18.23e^{-6.0 \times 10^{-5}t} + 7.82e^{-6.8 \times 10^{-5}t} \right] z^{0.825} \\ &+ \left[1 - 19.51e^{-5.4 \times 10^{-5}t} + 26.33e^{-6.0 \times 10^{-5}t} - 7.82e^{-6.8 \times 10^{-5}t} \right] z^{0.375} \end{aligned} \quad (26)$$

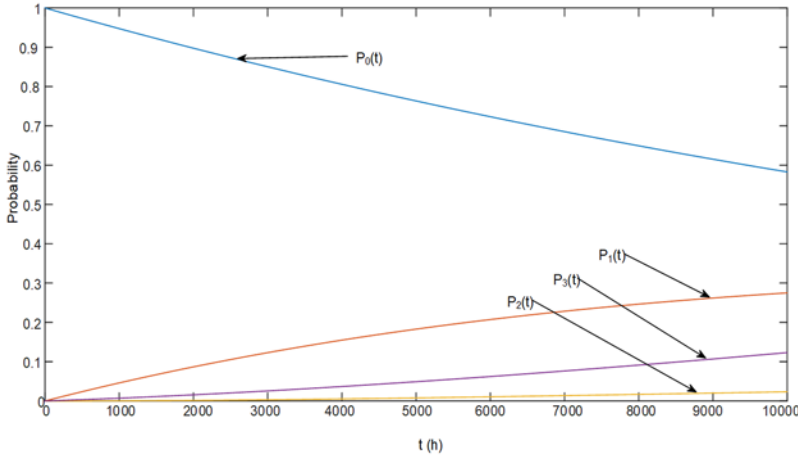


Fig. 14. The probability curves of the pump states

3.2.2. Servo valve

The servo valve is the control component in DHAS, which receives the command from the actuator control electronics (ACE) through the aviation bus. The power output of the servo valve is influenced by the command signal i_c from the ACE (externally) and mechanical degradation (internally). The schematic representation of the servo valve shown in Fig. 15 indicates the information flow and hydraulic power which together determine the power output of the servo valve.

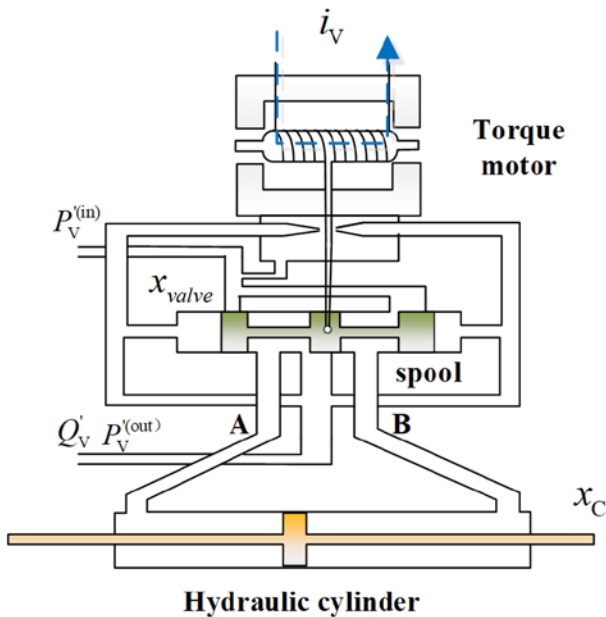


Fig. 15. Control current and power output of the servo valve

The servo valve consists of four main parts connected in series: electrical-mechanical conversion, mechanical-hydraulic conversion, hydraulic amplifier and feedback device. The failure of a single sub-assembly will lead to the failure of the entire servo valve. Each part's degradation/failure/repair behavior contributes to the mechanical states of the servo valve.

The PTE of servo valve can be formulated as:

$$\left\{ \begin{aligned} \eta_V &= \frac{W_V^{(out)}}{W_V^{(in)}} \\ W_V^{(out)} &= P_L \cdot Q_L = P_L \cdot C_q \cdot C_W \cdot K_V \cdot i_V \cdot \sqrt{\frac{1}{\rho} (P_{sys} - P_L)} \\ W_V^{(in)} &= W_P^{(out)} = P_{sys} \cdot Q_{sys} \end{aligned} \right. \quad (27)$$

in which, P_L and Q_L are the load pressure and load flow rate, respectively, which are directly related to the actual load. P_{sys} and Q_{sys} are the output pressure and output flow rate of the hydraulic pump. C_q, C_W, K_V are discharge coefficient of a servo valve, a gradient of valve orifice and amplification coefficient of servo valve respectively, ρ is density of hydraulic oil, which can be assumed to be a constant during operation, i_V is the controlled signal by actuator control electronics.

Given load pressure P_L , the PTE of servo valve η_V is determined by both control current states and mechanical states of the servo valve, i.e. $\eta_V = \eta_V^{(i_c)} \cdot \eta_V^{(M)}$, where $\eta_V^{(i_c)}$ indicates the control efficiency and $\eta_V^{(M)}$ indicates the mechanical efficiency.

The attenuation is inevitable in the process of control current of i_V transmission, which influences the output flow rate of servo valve. To simplify analysis, $\eta_V^{(i_c)} = [\eta_V^{(i_c)(0)}, \eta_V^{(i_c)(1)}, \eta_V^{(i_c)(2)}, \eta_V^{(i_c)(3)}]^T = [1.0, 0.8, 0.3, 0]^T$ is used to characterize the actual effects of different attenuation rates of control current acting on the efficiency of servo valve, and $P_V^{(i_c)} = [P_V^{(i_c)(0)}, P_V^{(i_c)(1)}, P_V^{(i_c)(2)}, P_V^{(i_c)(3)}]^T = [0.864, 0.118, 0.016, 0.002]^T$ is given to denote the corresponding probabilities that control current has different attenuation rates. Therefore, the sub-PTE model of servo valve which is linked with control current part, $PTU(\eta_V^{(i_c)}, P_V^{(i_c)})$, can be written as:

$$\begin{aligned} PTU(\eta_V^{(i_c)}, P_V^{(i_c)}) &= P_V^{(i_c)(0)} z^{\eta_V^{(i_c)(0)}} + P_V^{(i_c)(1)} z^{\eta_V^{(i_c)(1)}} + P_V^{(i_c)(2)} z^{\eta_V^{(i_c)(2)}} + P_V^{(i_c)(3)} z^{\eta_V^{(i_c)(3)}} \\ &= 0.864z^1 + 0.118z^{0.8} + 0.016z^{0.3} + 0.002z^0 \end{aligned} \quad (28)$$

Similar to hydraulic pump, wear between spool and sleeves in servo valve will reduce the output flow rate, and then reduce the mechanical efficiency $\eta_V^{(M)}$. According to the actual value of $\eta_V^{(M)}$ the mechanical states of the servo valve are divided into four discrete cases, i.e.:

$$s_V^{(M)} = \begin{cases} s_{V0} & \eta_V^{(M)(0)} \in [0.5, 0.667] \\ s_{V1} & \eta_V^{(M)(1)} \in [0.35, 0.5] \\ s_{V2} & \eta_V^{(M)(2)} \in [0.2, 0.35] \\ s_{V3} & \eta_V^{(M)(3)} \in [0, 0.2] \end{cases} \quad (29)$$

For a servo valve, the maximum mechanical efficiency can be 0.667 in the engineering field. When $\eta_V^{(M)} \in [0.5, 0.667]$, the servo valve operates very well, and s_{V0} is named as the normal state. With the increase of internal wear, the value of $\eta_V^{(M)}$ decreases into the interval of $[0.35, 0.5]$. In this case, the servo valve operates well despite the small amount of wear, so s_{V1} is named as the light degradation state. The value of $\eta_V^{(M)}$ enters into the interval of $[0.2, 0.35]$ with

$$\begin{aligned}
 \text{PTU}(\eta_V, A_V, P_V(t)) &= \text{PTU}_V^{iv}(\eta_V^{(iv)}, P_V^{(iv)}) \otimes \text{PTU}(\eta_V^{(M)}, A_V, P_V^{(M)}(t)) \\
 &= P_V^{iv(0)} P_V^{M(0)}(t) z^{\eta_V^{iv(0)} \eta_V^{M(0)}} + P_V^{iv(0)} P_V^{M(1)}(t) z^{\eta_V^{iv(0)} \eta_V^{M(1)}} + P_V^{iv(0)} P_V^{M(2)}(t) z^{\eta_V^{iv(0)} \eta_V^{M(2)}} + P_V^{iv(0)} P_V^{M(3)}(t) z^{\eta_V^{iv(0)} \eta_V^{M(3)}} \\
 &\quad + P_V^{iv(1)} P_V^{M(0)}(t) z^{\eta_V^{iv(1)} \eta_V^{M(0)}} + P_V^{iv(1)} P_V^{M(1)}(t) z^{\eta_V^{iv(1)} \eta_V^{M(1)}} + P_V^{iv(1)} P_V^{M(2)}(t) z^{\eta_V^{iv(1)} \eta_V^{M(2)}} + P_V^{iv(1)} P_V^{M(3)}(t) z^{\eta_V^{iv(1)} \eta_V^{M(3)}} \\
 &\quad + P_V^{iv(2)} P_V^{M(0)}(t) z^{\eta_V^{iv(2)} \eta_V^{M(0)}} + P_V^{iv(2)} P_V^{M(1)}(t) z^{\eta_V^{iv(2)} \eta_V^{M(1)}} + P_V^{iv(2)} P_V^{M(2)}(t) z^{\eta_V^{iv(2)} \eta_V^{M(2)}} + P_V^{iv(2)} P_V^{M(3)}(t) z^{\eta_V^{iv(2)} \eta_V^{M(3)}} \\
 &\quad + P_V^{iv(3)} P_V^{M(0)}(t) z^{\eta_V^{iv(3)} \eta_V^{M(0)}} + P_V^{iv(3)} P_V^{M(1)}(t) z^{\eta_V^{iv(3)} \eta_V^{M(1)}} + P_V^{iv(3)} P_V^{M(2)}(t) z^{\eta_V^{iv(3)} \eta_V^{M(2)}} + P_V^{iv(3)} P_V^{M(3)}(t) z^{\eta_V^{iv(3)} \eta_V^{M(3)}}
 \end{aligned} \tag{33}$$

continuous accumulation of inner wear, the performance of servo valve degrades obviously, thus s_{V2} is named as serious degradation state.

Once $\eta_V^{(M)} < 0.2$, the servo valve will be regarded as failed. Median value of each interval is utilized as the indicator of $\eta_V^{(M)}$, and we get $\eta_V^{(M)} = [\eta_V^{M(0)} \ \eta_V^{M(1)} \ \eta_V^{M(2)} \ \eta_V^{M(3)}]^T = [0.5835 \ 0.425 \ 0.275 \ 0.1]^T$.

Given the reliability parameters of servo valve as listed in Table 4, the probabilities that the servo valve stays in $s_V^{(M)}$ can be obtained with the similar GSPN model and Markov model of hydraulic pump shown in Fig. 13.

Table 4. Parameters of servo valve model

Parameter	Value	Parameter	Value
$P(t_{Vi1})$	0.9	$P(t_{Vi2})$	0.5
$P(t_{Vi3})$	0.1	$P(t_{Vi4})$	0.5
λ_{V1}	$8.6 \times 10^{-5} / h$	λ_{V2}	$9.0 \times 10^{-5} / h$
λ_{V3}	$9.8 \times 10^{-5} / h$		

According to GSPN model, the state transition matrix of servo valve, A_V , can be written as:

$$A_V = \begin{bmatrix} -8.6 \times 10^{-5} & 0 & 0 & 0 \\ 7.74 \times 10^{-5} & -9.0 \times 10^{-5} & 0 & 0 \\ 0 & 4.5 \times 10^{-5} & -9.8 \times 10^{-5} & 0 \\ 9 \times 10^{-6} & 4.5 \times 10^{-5} & 9.8 \times 10^{-5} & 0 \end{bmatrix} \tag{30}$$

Then, the probabilities of mechanical states of the servo valve are obtained as:

Then, the probabilities $P_V^{(M)}(t)$ of mechanical states of the servo valve are obtained as:

$$P_V^{(M)}(t) = \begin{bmatrix} P_V^{M(0)}(t) \\ P_V^{M(1)}(t) \\ P_V^{M(2)}(t) \\ P_V^{M(3)}(t) \end{bmatrix} = \begin{bmatrix} e^{-8.6 \times 10^{-5} t} \\ 19.35 \times (e^{-8.6 \times 10^{-5} t} - e^{-9.0 \times 10^{-5} t}) \\ 72.56 e^{-8.6 \times 10^{-5} t} - 108.84 e^{-9.0 \times 10^{-5} t} + 36.28 e^{-9.8 \times 10^{-5} t} \\ 1 - 92.91 e^{-8.6 \times 10^{-5} t} + 128.19 e^{-9.0 \times 10^{-5} t} - 36.28 e^{-9.8 \times 10^{-5} t} \end{bmatrix} \tag{31}$$

Therefore, the sub-PTE model of servo valve relating with mechanical states part, $\text{PTU}(\eta_V^{(M)}, A_V, P_V^{(M)}(t))$, can be written as:

$$\begin{aligned}
 \text{PTU}(\eta_V^{(M)}, P_V^{(M)}(t)) &= p_V^{M(0)} z^{\eta_V^{M(0)}} + p_V^{M(1)} z^{\eta_V^{M(1)}} + p_V^{M(2)} z^{\eta_V^{M(2)}} + p_V^{M(3)} z^{\eta_V^{M(3)}} \\
 &= e^{-8.6 \times 10^{-5} t - 0.5835} + 19.35 \times (e^{-8.6 \times 10^{-5} t} - e^{-9.0 \times 10^{-5} t}) z^{0.425} \\
 &\quad + [72.56 e^{-8.6 \times 10^{-5} t} - 108.84 e^{-9.0 \times 10^{-5} t} + 36.28 e^{-9.8 \times 10^{-5} t}] z^{0.275} \\
 &\quad + [1 - 92.91 e^{-8.6 \times 10^{-5} t} + 128.19 e^{-9.0 \times 10^{-5} t} - 36.28 e^{-9.8 \times 10^{-5} t}] z^{0.1}
 \end{aligned} \tag{32}$$

The complete PTE model of servo valve can be written as Equation (33) [above].

3.2.3. Hydraulic cylinder

Fig. 16 shows the inner structure of a hydraulic cylinder in which the leakage due to the friction and wear is the main failure behavior. Since the wear and tear between the piston and cylinder are progressive, the multiple degradation states based on a GSPN model can be used to establish the reliability model.

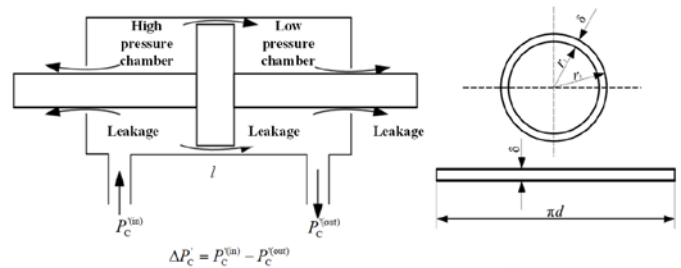


Fig. 16. Working principle of hydraulic cylinder

The output power of hydraulic cylinder is:

$$W_C^{(out)} = F_L \cdot V = \eta_C \cdot P_L \cdot Q_L = \eta_C \cdot W_V^{(out)} \tag{34}$$

where η_C is volumetric efficiency of hydraulic cylinder.

The value of η_C is determined by wear status of the hydraulic cylinder. According to the actual value of η_C , the states of the cylinder are divided into four discrete cases mentioned above, i.e.:

$$s_C = \begin{cases} s_{C0} & \eta_C^{(0)} \in [0.95, 1] \\ s_{C1} & \eta_C^{(1)} \in [0.85, 0.95] \\ s_{C2} & \eta_C^{(2)} \in [0.75, 0.85] \\ s_{C3} & \eta_C^{(3)} \in [0, 0.75] \end{cases} \tag{35}$$

Table 5. Parameters of the hydraulic cylinder model

Parameter	Value	Parameter	Value
$P(t_{Ci1})$	0.8	$P(t_{Ci2})$	0.6
$P(t_{Ci3})$	0.2	$P(t_{Ci4})$	0.4
λ_{C1}	$2.2 \times 10^{-6} / \text{h}$	λ_{C2}	$3.6 \times 10^{-6} / \text{h}$
λ_{C3}	$6.7 \times 10^{-6} / \text{h}$		

Median value of each interval is used as the indicator of η_C , and we can get $\eta_C = [\eta_C^{(0)} \ \eta_C^{(1)} \ \eta_C^{(2)} \ \eta_C^{(3)}]^T = [0.975 \ 0.9 \ 0.8 \ 0.375]^T$.

Given the reliability parameters of hydraulic cylinder as listed in Table 5, the probabilities that the hydraulic cylinder stays in s_C can be obtained with the similar GSPN model and Markov model same to hydraulic pump shown in Fig. 13.

According to GSPN model, the state transition matrix of hydraulic pump A_C can be written as:

$$A_C = \begin{bmatrix} -2.2 \times 10^{-6} & 0 & 0 & 0 \\ 1.76 \times 10^{-6} & -3.6 \times 10^{-6} & 0 & 0 \\ 0 & 2.16 \times 10^{-6} & -6.7 \times 10^{-6} & 0 \\ 4.4 \times 10^{-7} & 0 & 6.7 \times 10^{-6} & 0 \end{bmatrix} \quad (36)$$

Then, the steady probabilities $P_C(t)$ of hydraulic cylinder are listed as:

$$P_C(t) = \begin{bmatrix} P_C^{(0)}(t) \\ P_C^{(1)}(t) \\ P_C^{(2)}(t) \\ P_C^{(3)}(t) \end{bmatrix} = \begin{bmatrix} e^{-2.2 \times 10^{-6} t} \\ 1.26 \times (e^{-2.2 \times 10^{-6} t} - e^{-3.6 \times 10^{-6} t}) \\ 0.60 e^{-2.2 \times 10^{-6} t} - 0.87 e^{-3.6 \times 10^{-6} t} + 0.27 e^{-6.7 \times 10^{-6} t} \\ 1 - 2.86 e^{-2.2 \times 10^{-6} t} + 2.13 e^{-3.6 \times 10^{-6} t} - 0.27 e^{-6.7 \times 10^{-6} t} \end{bmatrix} \quad (37)$$

Therefore, for a hydraulic cylinder, the stochastic power transmission model, $PTU(\eta_C, A_C, P_C(t))$, can be written as:

$$\begin{aligned} PTU(\eta_C, A_C, P_C(t)) &= P_C^{(0)}(t) z^{\eta_C^{(0)}} + P_C^{(1)}(t) z^{\eta_C^{(1)}} + P_C^{(2)}(t) z^{\eta_C^{(2)}} + P_C^{(3)}(t) z^{\eta_C^{(3)}} \\ &= e^{-2.2 \times 10^{-6} t} z^{0.975} + 1.26 \times (e^{-2.2 \times 10^{-6} t} - e^{-3.6 \times 10^{-6} t}) z^{0.9} \\ &\quad + \left[0.60 e^{-2.2 \times 10^{-6} t} - 0.87 e^{-3.6 \times 10^{-6} t} + 0.27 e^{-6.7 \times 10^{-6} t} \right] z^{0.8} \\ &\quad + \left[1 - 2.86 e^{-2.2 \times 10^{-6} t} + 2.13 e^{-3.6 \times 10^{-6} t} - 0.27 e^{-6.7 \times 10^{-6} t} \right] z^{0.375} \end{aligned} \quad (38)$$

3.2.4. Control surface

Control surface is one of the terminal customers, so the output power of DHAS is used to drive the control surface to implement the aircraft flight control. To simplify the PTE-based model, we defined the mechanical efficiency of the control surface as $\eta_{sur} = 0.95$. Its mechanical failure rate $\lambda_{sur} = 2.2 \times 10^{-6} / \text{h}$ is selected from Table 1, then

we can get the reliability of control surface as $P_{sur}(t) = e^{-3.2 \times 10^{-6} t}$, therefore:

$$PTU(\eta_{sur}, P_{sur}) = e^{-3.2 \times 10^{-6} t} \times z^{0.95} \quad (39)$$

3.2.5. Engine accessory gearbox

The aircraft engine provides initial power input for aircraft power supply and actuation system through engine accessory gearbox. The mechanical energy is provided by the engine accessory gearbox. Similar with the control surface, it is supposed that the mechanical efficiency of the accessory gearbox is $\eta_G = 0.853$, and the reliability of accessory gearbox is $P_G(t) = e^{-3.0 \times 10^{-6} t}$, then the PTE-based model of engine accessory gearbox is obtained as:

$$PTU(\eta_G, P_G) = e^{-3.0 \times 10^{-6} t} \cdot z^{0.853} \quad (40)$$

3.3. PTE-based reliability model of DHAS

The PTE-based model for single hydraulic actuation system (HAS) is given by:

$$\begin{aligned} HAS(\eta_{HAS_1}, P_{HAS_1}(t)) &= (\eta_{P_1}, A_{P_1}, P_{P_1}(t)) \otimes (\eta_{V_1}, A_{V_1}, P_{V_1}(t)) \otimes (\eta_{C_1}, A_{C_1}, P_{C_1}(t)) \\ &= \sum_{i=0}^3 \sum_{j=0}^{15} \sum_{k=0}^3 P_P^{(i)}(t) P_V^{(j)}(t) P_C^{(k)}(t) \cdot z^{\eta_P^{(i)} \eta_V^{(j)} \eta_C^{(k)}} \\ HAS(\eta_{HAS_2}, P_{HAS_2}(t)) &= (\eta_{P_2}, A_{P_2}, P_{P_2}(t)) \otimes (\eta_{V_2}, A_{V_2}, P_{V_2}(t)) \otimes (\eta_{C_2}, A_{C_2}, P_{C_2}(t)) \\ &= \sum_{i=0}^3 \sum_{j=0}^{15} \sum_{k=0}^3 P_P^{(i)}(t) P_V^{(j)}(t) P_C^{(k)}(t) \cdot z^{\eta_P^{(i)} \eta_V^{(j)} \eta_C^{(k)}} \end{aligned} \quad (41)$$

The complete PTE-based model of DHAS is composed of dual HASs, engine accessory gearbox and control surface, thus:

$$\begin{aligned} DHAS(\eta_{DHAS}, P_{DHAS}(t)) &= (\eta_G, P_G(t)) \otimes (HAS(\eta_{HAS_1}, P_{HAS_1}(t)) \otimes HAS(\eta_{HAS_2}, P_{HAS_2}(t))) \otimes (\eta_{sur}, P_{sur}(t)) \\ &= (\eta_G, P_G(t)) \otimes \left(\sum_{i=0}^3 \sum_{j=0}^{15} \sum_{k=0}^3 P_P^{(i)}(t) P_V^{(j)}(t) P_C^{(k)}(t) z^{\frac{\eta_{HAS_1}^{(i)} \eta_{HAS_2}^{(j)}}{2}} \right) \otimes (\eta_{sur}, P_{sur}(t)) \\ &= e^{-2.2 \times 10^{-6} t} \cdot z^{0.853} \otimes \left(\sum_{i=0}^3 \sum_{j=0}^{15} \sum_{k=0}^3 P_P^{(i)}(t) P_V^{(j)}(t) P_C^{(k)}(t) z^{\frac{\eta_{HAS_1}^{(i)} \eta_{HAS_2}^{(j)}}{2}} \right) \otimes e^{-2.2 \times 10^{-6} t} \cdot z^{0.95} \end{aligned} \quad (42)$$

Given the power input of DHAS, $W_{DHAS}^{(in)} = 66.5 \text{ kW}$, $DHAS(W_{DHAS}^{(out)}, P_{DHAS}(t))$ can be expressed as:

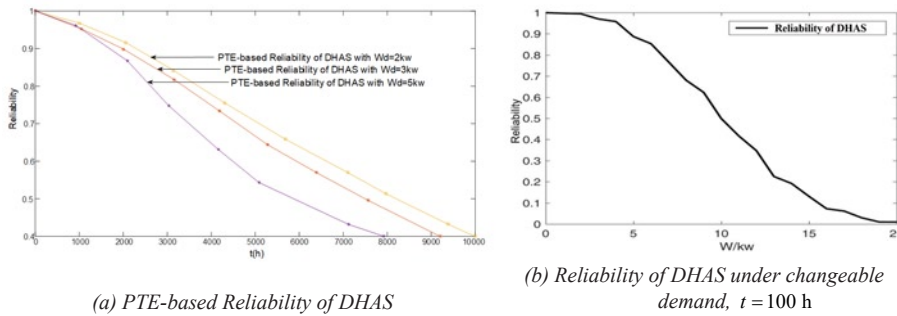
$$DHAS(W_{DHAS}^{(out)}, P_{DHAS}(t)) = e^{-2.2 \times 10^{-6} t} \cdot z^{56.72} \otimes \left(\sum_{i=0}^3 \sum_{j=0}^{15} \sum_{k=0}^3 P_P^{(i)}(t) P_V^{(j)}(t) P_C^{(k)}(t) z^{\frac{\eta_{HAS_1}^{(i)} \eta_{HAS_2}^{(j)}}{2}} \right) \otimes e^{-2.2 \times 10^{-6} t} \cdot z^{0.95} \quad (43)$$

According to Eq. (43), we can get combination items of $(W_{DHAS}^{(out)})^i P_{DHAS}^{(i)}(t)$, $i = 0, 1, 2, \dots, n_{DHAS} - 1$. Then the PTE-based reliability model of DHAS can be written as:

$$R^p(t | W_{DHAS}^{(out)} \geq W^{(d)}) = \sum_{i=1}^m \left\{ P_{DHAS}^{(i)}(t) \cdot 1(W_{DHAS}^{(out)i} - W^{(d)} \geq 0) \right\} \quad (44)$$

where $W^{(d)}$ is actual control surface driving power demand.

From Eq. (43) and Eq. (44), we can calculate the reliability of DHAS with the constant demand of $W^{(d)} \in [0,20]$ (kW) as shown in Fig. 17.



(a) PTE-based Reliability of DHAS
 (b) Reliability of DHAS under changeable demand, $t = 100$ h

Fig. 17. PTE-based Reliability curves of DHAS

The power transfer process of a component is different from fault mode transmission process, which will pose a different impact on DHAS. In addition, the variable demand is another key factor that reflects the performance of DHAS. From Fig. 17 (b), it can be concluded that the reliability of DHAS decreases as the demand of the control surface increases.

3.3.1. Reliability analysis of DHAS under variable power demands

Since the power requirements of aileron actuation system are different in different stage of flight profiles, the power consumption at different flight stage is also various. Table 6 shows the power requirement at conventional flight profile of an aircraft, which includes taxiing, taking off, climbing, cruising, descending and landing.

Table 6 shows the different power demand of each flight profile, in which power means the power requirement at different flight stages and proportion indicates the proportion of power at different stages to the power of whole flight profile. It shows that the more power the demand needs in the flight profile, the better the maneuverability is. We established the PTE-based reliability model at different stages for DHAS and calculated its reliability shown in Fig. 18.

Table 6. Power consumption under 6 flight profile and duration of an aileron [20]

Phase	Taxing	Taking off	Climbing	Cruising	Descending	Landing
Power (kW)	0.98	1.71	1.31	1.25	1.51	2.35
Proportion	0.03	0.02	0.04	0.85	0.04	0.02

Fig. 18 shows that the reliability diversification is sensitive to the large power requirement profiles such as taking off, descending and landing, so the power-based reliability of DHAS needs to be seriously considered in such operational condition. However, the power-based reliability has little change in some small power demand such as cruise and taxiing.

Table 7. The flow rate of pump in different flight stage [20]

Flight stage	Pitch check	Roll check	Yaw check	Take off start	Stop taking off	Take off	Climbing	Cruise	Emergency decline
Flow rate (gpm)	6.33	11.7	9.47	12.27	21.84	4.45	4.45	4.55	7.04
Flight stage	Air collision	Decline	Turbulence	Go around	Spoiler unfolding	Landing brake	Landing run	Stop landing	Slide
Flow rate (gpm)	7.21	4.55	7.9	10.45	19.74	6.65	21.94	4.55	6.15

3.3.2. Reliability analysis of DHAS with the change of hydraulic pump's flow rate

Hydraulic pump is the key component of power supply system of DHAS. The pump maintains the constant pressure while changes the flow rate accordingly to meet the mission demand. The flow rate supply of a kind of hydraulic pump, during different flight stages, is listed in Table 7.

Applying the numerical procedure for hydraulic pump presented in Section 3.2.1, the DHAS reliability curve can be obtained shown in Fig. 19 with the changes of flow rate.

In Fig. 19, the reliability of DHAS exits a trough in the middle of power requirement and corresponding flow rate, which means that DHAS cannot drive the control surface according to the control command even when

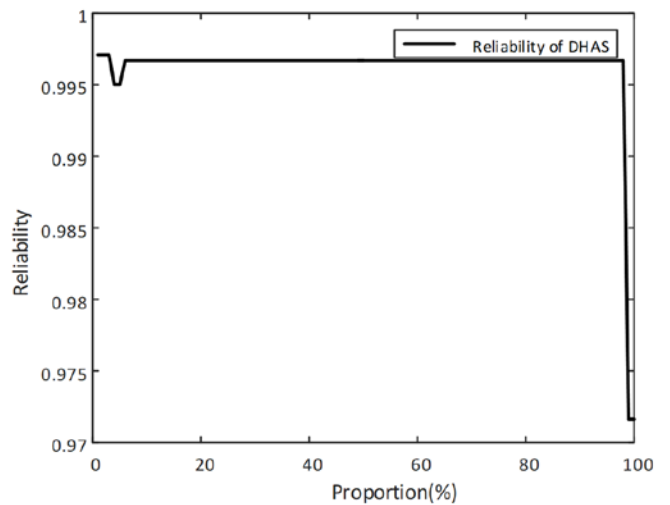


Fig. 18. Reliability of aileron driven by DHAS under flight profile, total $t = 100$ h

DHAS can provide partial power. With the power approaches the power requirement, the reliability increases and keeps at a high level for a long time. In such condition, aircraft can operate in satisfied performance under enough power supply. In addition, the reliability of DHAS keeps at a high level when the hydraulic pump changes its flow rate to meet the power supply needs according to the flight command.

If we observe a two-dimensional view of the three-dimensional reliability curve, we can see that the different variation tendency with the change of pump flow rate or the change of power requirement. The ideal situation is the reliability keeping high with appropriate power requirement and appropriate power supply. We can get the optimal value with the reliability as a

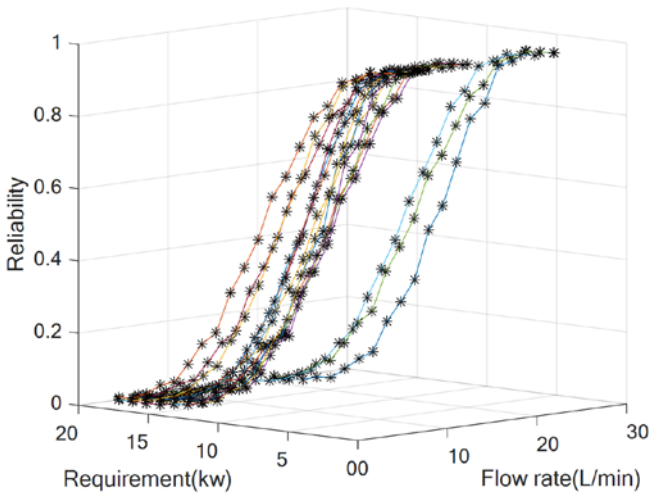


Fig. 19. Reliability of DHAS with the changing flow rate of pump under changing demand

objective function, the power requirement and pump flow rate supply as a restriction. It also indicates that the PTE-based reliability model of DHAS can provide integrated evaluation on DHAS task completion effectively considering reliability and power changes.

3.3.3. Reliability analysis of DHAS with different hydraulic pump degradation rates

In order to analyze the influence of hydraulic pump degradation to DHAS reliability in the GSPN model, we change the degrading failure rate λ_{p1} and calculate the reliability of DHAS under different power requirements in $t = 100h$ as shown in Fig. 20.

Fig. 20 gives the sensitivity analysis of PTE-based reliability of DHAS to degradation rate of hydraulic pump. Fig. 20. (a) indicates that the reliability of DHAS is less than 0.01% under terminal power demand of 1 kW while the degradation rate of pump changes from $0.1 \times 10^{-4} / h$ to $5 \times 10^{-4} / h$. Fig. 20 (b) shows the variation of the PTE-based reliability of DHAS reaches 5.5% with terminal power demand ranging from 1 kW to 5 kW while the degradation rate changes from $0.1 \times 10^{-5} / h$ to $5 \times 10^{-5} / h$. Fig. 20 (c) expresses the variation of the PTE-based reliability of DHAS reaches 18% under terminal power demand as 20 kW. So PTE-based reliability is sensitive to the terminal power requirements.

3.3.4. Comparison between PTE-based reliability and traditional reliability of DHAS

In order to verify the effectiveness of the proposed reliability analysis, we compare the PTE-based reliability model proposed in this paper with the traditional reliability model based on RBD for DHAS. The reliability curve under proposed method and the RBD with the parameters of Table 1 is shown in Fig. 21.

In Fig. 21, the blue line means the reliability based on RBD, the yellow line indicates the reliability under 2 kW power requirement, the red line is the reliability under 3 kW power demand and the purple line expresses the reliability under 5 kW power demand. It is apparently that the traditional reliability of DHAS is higher than PTE-based reliability if we don't consider the power requirement. However, DHAS is the fast response system that needs enough power supply to implement large maneuvering flight, so it is necessary to consider the dynamic performance related to the power supply. From the reliability curve of different power requirements in Fig. 21, it indicates that the PTE-reliability is closely related to the power demands. When the response time is not very high, the power demand is small and the PTE-based reliability decreases gradually. When the DHAS ne-

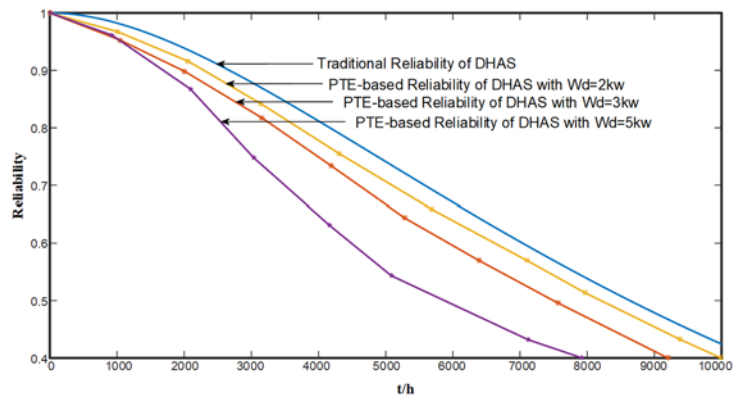
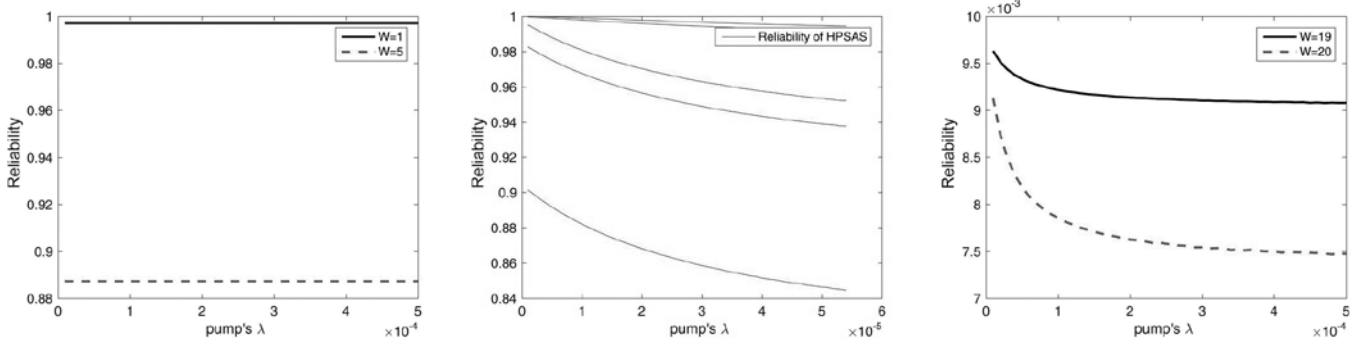


Fig. 21. Reliability comparison between PTE-based model and BRD model

eds fast maneuvering, PTE-based reliability drops quickly. Hence, the PTE-based reliability is the appropriate reliability model to evaluate its reliability under satisfied dynamic performance.

4. Conclusion

This paper proposes a PTE-based reliability model considering the PTE and degradation process of component and system. In PTE-based reliability model, the power requirement, power capacity and



(a) $W^{(d)} = 1kW, 5kW$ (b) $W^{(d)} = 1kW \sim 5kW$ (c) $W^{(d)} = 19kW, 20kW$

Fig. 20. Reliability comparison of DHAS with changing physical degradation rate of pump

PTE are randomized to describe its reliability. Due to the inherent degradation of PTS, this paper presents a stochastic power transmission model under multiple degradation states, utilizing the GSPN and UGF to calculate the power-based reliability with specific power requirement. DHAS is taken as a case to show how to carry out the PTE-reliability evaluation for dynamic performance related system. Based on the PTE-reliability model of hydraulic pump, servo valve, hydraulic cylinder and control surface, this paper establishes the PTE-reliability model of DHAS and gives the comparison between the traditional reliability model and the proposed method. The results

indicate that the PTE-based reliability model is more suitable for the system requiring dynamic performance under enough power supply. PTE-based reliability model can characterize the essential reliability characteristics of DHAS accurately under multiple power demands and performance requirements.

Acknowledgement

The research work is supported by the National Natural Science Foundation of China (Grants No. 51875014, 51620105010, 51575019).

References

- Benabid R, Merrouche D, Bourenane A, and Alzbutas R. Reliability Assessment of Redundant Electrical Power Supply Systems using Fault Tree Analysis, Reliability Block Diagram, and Monte Carlo Simulation Methods. 2018 International Conference on Electrical Sciences and Technologies in Maghreb (CISTEM). IEEE 2018: 1-7, <https://doi.org/10.1109/CISTEM.2018.8613431>.
- Bennett J W, Atkinson G J, Mecrow B C, et al. Fault-tolerant design considerations and control strategies for aerospace drives. IEEE Transactions on Industrial Electronics 2011; 59(5): 2049-2058, <https://doi.org/10.1109/TIE.2011.2159356>.
- Cepin, M. Evaluation of the importance factors of the power plants within the power system reliability evaluation. Eksploatacja i Niezawodność - Maintenance and Reliability 2019; 21(4): 631-637, <https://doi.org/10.17531/ein.2019.4.12>.
- Chakraborty I, Trawick D R, Mavris D N, et al. A requirements-driven methodology for integrating subsystem architecture sizing and analysis into the conceptual aircraft design phase. 14th AIAA Aviation Technology, Integration, and Operations Conference 2014: 3012, <https://doi.org/10.2514/6.2014-3012>.
- Cui X, Wang S, Li T, and Shi J. System Reliability Assessment Based on Energy Dissipation: Modeling and Application in Electro-Hydrostatic Actuation System. Energies 2019; 12(18): 3572, <https://doi.org/10.3390/en12183572>.
- Dong W, Liu S, Tao L, Cao Y, and Fang Z. Reliability variation of multi-state components with inertial effect of deteriorating output performances. Reliability Engineering & System Safety 2019 186: 176-185, <https://doi.org/10.1016/j.res.2019.02.018>.
- Hespanha J P. Modeling and analysis of networked control systems using stochastic hybrid systems. Annual Reviews in Control 2014; 38(2): 155-170, <https://doi.org/10.1016/j.arcontrol.2014.09.001>.
- Hirsch W M, Meisner M, Boll C. Cannibalization in multicomponent systems and the theory of reliability. Naval Research Logistics Quarterly 1968; 15(3): 331-360, <https://doi.org/10.1002/nav.3800150302>.
- IEC, Functional Safety of Electrical/Electronic/Programmable Electronic Safety Related Systems, IEC 61508, 2000.
- Jafary B, Fiondella L. A universal generating function-based multi-state system performance model subject to correlated failures. Reliability Engineering & System Safety 2016; 152: 16-27, <https://doi.org/10.1016/j.res.2016.02.004>.
- Jia H, Levitin G, Ding Y, et al. Reliability analysis of standby systems with multi-state elements subject to constant transition rates. Quality and Reliability Engineering International 2019; 35(1): 318-328, <https://doi.org/10.1002/qre.2401>.
- Lee S H. Reliability evaluation of a flow network. IEEE Transactions on Reliability 1980; 29(1): 24-26, <https://doi.org/10.1109/TR.1980.5220695>.
- Levitin G. The universal generating function in reliability analysis and optimization. London: Springer, 2005.
- Li S, Zhu Z C, Lu H, Shen G. A system reliability-based design optimization for the scraper chain of scraper conveyors with dependent failure modes. Eksploatacja i Niezawodność - Maintenance and Reliability 2019; 21(3): 392-402, <https://doi.org/10.17531/ein.2019.3.5>.
- Li X Y, Huang H Z, Li Y F, et al. Reliability assessment of multi-state phased mission system with non-repairable multi-state components. Applied Mathematical Modelling 2018; 61: 181-199, <https://doi.org/10.1016/j.apm.2018.04.008>.
- Lin Y H, Li Y F, Zio E. Integrating random shocks into multi-state physics models of degradation processes for component reliability assessment. IEEE Transactions on Reliability 2014; 64(1): 154-166, <https://doi.org/10.1109/TR.2014.2354874>.
- Lin Y K. A simple algorithm for reliability evaluation of a stochastic-flow network with node failure. Computers & Operations Research 2001; 28(13): 1277-1285, [https://doi.org/10.1016/S0305-0548\(00\)00039-3](https://doi.org/10.1016/S0305-0548(00)00039-3).
- Lisnianski A, Frenkel I, Ding Y. Multi-state system reliability analysis and optimization for engineers and industrial managers. Springer Science & Business Media 2010, <https://doi.org/10.1007/978-1-84996-320-6>.
- Lisnianski A, Levitin G. Multi-state system reliability: assessment, optimization and applications. World Scientific Publishing Company 2003, <https://doi.org/10.1142/5221>.
- Ma Z, Wang S, Zhang C, et al. A Load Sequence Design Method for Hydraulic Piston Pump Based on Time-Related Markov Matrix. IEEE Transactions on Reliability 2018; 67(3): 1237-1248, <https://doi.org/10.1109/TR.2018.2830330>.
- Malinowski J. Reliability analysis of a flow network with a series-parallel-reducible structure. IEEE Transactions on Reliability 2015; 65(2): 851-859, <https://doi.org/10.1109/TR.2015.2499962>.
- Peng H, Feng Q and Coit D W. Reliability and maintenance modeling for systems subject to multiple dependent competing failure processes. IIE transactions 2010; 43(1): 12-22, <https://doi.org/10.1080/0740817X.2010.491502>.
- Qin J L, Niu Y G, Li Z. A combined method for reliability analysis of multi-state system of minor-repairable components. Eksploatacja i Niezawodność - Maintenance and Reliability 2016; 18(1): 80-88, <https://doi.org/10.17531/ein.2016.1.11>.
- Raveendran V, Andresen M and Liserre M. Improving onboard converter reliability for more electric aircraft with lifetime-based control. IEEE Transactions on Industrial Electronics 2019; 66(7): 5787-5796, <https://doi.org/10.1109/TIE.2018.2889626>.
- Rosero J A, Ortega J A, Aldabas E, et al. Moving towards a more electric aircraft. IEEE Aerospace and Electronic Systems Magazine 2007; 22(3): 3-9, <https://doi.org/10.1109/MAES.2007.340500>.
- Steffen T, Schiller F, Blum M, and Dixon R. Analysing the reliability of actuation elements in series and parallel configurations for high-redundancy actuation. International Journal of Systems Science 2013; 44(8): 1504-1521, <https://doi.org/10.1080/00207721.2012.659694>.

27. Ushakov I A. Optimal standby problems and a universal generating function. Soviet journal of computer and systems sciences, 1987; 25(4): 79-82.
28. Wang K, Wang S, Shi J. A novel multi-state reliability assessment model for servo HA/EHA system via universal generating function. 2017 IEEE International Conference on Mechatronics and Automation (ICMA). IEEE 2017: 1918-1923, <https://doi.org/10.1109/ICMA.2017.8016111>.
29. Wang S, Cui X, Shi J, Tomovic M M, and Jiao Z. Modeling of reliability and performance assessment of a dissimilar redundancy actuation system with failure monitoring. Chinese Journal of Aeronautics 2016; 29(3): 799-813, <https://doi.org/10.1016/j.cja.2015.10.002>.
30. Wang W, Di Maio F, Zio E. Three-loop Monte Carlo simulation approach to Multi-State Physics Modeling for system reliability assessment. Reliability Engineering & System Safety 2017; 167: 276-289, <https://doi.org/10.1016/j.res.2017.06.003>.
31. Wang Y S, Fang X, Zhang C H , Chen X, Lu J Z. Lifetime prediction of self-lubricating spherical plain bearings based on physics-of-failure model and accelerated degradation test. Eksploatacja i Niezawodnosc - Maintenance and Reliability 2016; 18(4): 528-538, <https://doi.org/10.17531/ein.2016.4.7>.
32. Wu J, Yan S, Xie L, et al. Reliability apportionment approach for spacecraft solar array using fuzzy reasoning Petri net and fuzzy comprehensive evaluation. Acta Astronautica 2012; 76: 136-144, <https://doi.org/10.1016/j.actaastro.2012.02.023>.
33. Xu D, Feng Z, Sui S, and Lin Y. Reliability Assessment of Electro-hydraulic Actuator Control System Subject to Multi-Sources Degradation Processes. IEEE/ASME Transactions on Mechatronics 2019, <https://doi.org/10.1109/TMECH.2019.2953333>.
34. Yu H, Chu C, Châtelet È, et al. Reliability optimization of a redundant system with failure dependencies. Reliability Engineering & System Safety 2007; 92(12): 1627-1634, <https://doi.org/10.1016/j.res.2006.09.015>.
35. Zhang J, Qun C and Xu B. Analysis of the cylinder block tilting inertia moment and its effect on the performance of high-speed electro-hydrostatic actuator pumps of aircraft. Chinese Journal of Aeronautics 2018; 31(1): 169-177, <https://doi.org/10.1016/j.cja.2017.02.010>.
36. Zio E. An introduction to the basics of reliability and risk analysis. World scientific 2007, <https://doi.org/10.1142/6442>.
37. Zio E. Some Challenges and Opportunities in Reliability Engineering. IEEE Transactions on Reliability 2016; 65(4):1769-1782, <https://doi.org/10.1109/TR.2016.2591504>.

Xiaoyu CUI

School of Materials Science and Mechanical Engineering
Beijing Technology and Business University
100048, Beijing, China

Tongyang LI

China Civil Aviation Engineering Consulting Co., Ltd
100621, Beijing, China

Shaoping WANG

School of Automation Science and Electrical Engineering
Beihang University
100191, Beijing, China

Jian SHI

School of Automation Science and Electrical Engineering
Beihang University
100191, Beijing, China

Zhonghai MA

Beijing Key Laboratory of Advanced Manufacturing Technology
Beijing University of Technology
100124, Beijing, China

E-mails: xiaoyucui@btbu.edu.cn, soresun@buaa.edu.cn,
shaopingwang@vip.sina.com, shijian@buaa.edu.cn, zm@bjut.edu.cn
